

**SYNTHESIS AND CHARACTERISATION OF
Ni-Fe/ γ -Al₂O₃ BIMETALLIC CATALYST FOR HYDROGENATION OF
FATTY ACIDS**

WONG FARNG HUI

**A project report submitted in partial fulfilment of the
requirements for the award of the degree of
Bachelor of Engineering (Hons.) Chemical Engineering**

**Lee Kong Chian Faculty of Engineering and Science
Universiti Tunku Abdul Rahman**

April 2016

DECLARATION

I hereby declare that this project report is based on my original work except for citations and quotations which have been duly acknowledged. I also declare that it has not been previously and concurrently submitted for any other degree or award at UTAR or other institutions.

Signature : _____

Name : _____

ID No. : _____

Date : _____

APPROVAL FOR SUBMISSION

I certify that this project report entitled **“SYNTHESIS AND CHARACTERISATION OF Ni-Fe/ γ -Al₂O₃ BIMETALLIC CATALYST FOR HYDROGENATION OF FATTY ACIDS”** was prepared by **WONG FARNG HUI** has met the required standard for submission in partial fulfilment of the requirements for the award of Bachelor of Engineering (Hons.) Chemical Engineering at Universiti Tunku Abdul Rahman.

Approved by,

Signature : _____

Supervisor: Dr. Yap Yeow Hong

Date : _____

The copyright of this report belongs to the author under the terms of the copyright Act 1987 as qualified by Intellectual Property Policy of University Tunku Abdul Rahman. Due acknowledgement shall always be made of the use of any material contained in, or derived from, this report.

© 2016, Wong Farnng Hui. All right reserved.

Specially dedicated to
Dr. Yap Y.H., my family and friends

ACKNOWLEDGEMENTS

I would like to thank everyone who had contributed to the successful completion of this project. My deepest gratitude to my research supervisor Dr. Yap Yeow Hong for his invaluable advice, guidance and enormous patience throughout the development of this research.

In addition, I would also like to express my gratitude to my loving parent and friends who had helped and given me encouragement to persevere and complete this journey. Not to forget the dedicated lab officers who had generously helped facilitate the use of research labs and equipment.

**SYNTHESIS AND CHARACTERISATION OF
Ni-Fe/ γ -Al₂O₃ BIMETALLIC CATALYST FOR HYDROGENATION OF
FATTY ACIDS**

ABSTRACT

Oleochemicals are indispensable in production of various industrial and consumer goods such as lubricants, waxes, soaps and candles. Amidst the vast range of oleochemical processes, hydrogenation of fatty acids is particularly of high concern as it produces basic building blocks of oleochemicals such as stearic acid and palmitic acid that would be used in many downstream processes. The efficiency and effectiveness of hydrogenation process depends highly on the use of catalysts thus continuous efforts have been made to improve the catalyst technically and economically. Past research have found that platinum shows the best performance in hydrogenation but nickel catalyst remains the most popular choice for being way more economical with only slight compromise on catalytic performance. This project looks into the potential incorporation of iron into nickel catalyst in order to explore the possibilities of improving catalytic performance and lowering catalyst cost as iron is cheaper than nickel. This project consisted of two main steps: synthesis and characterisation. Charge enhanced dry impregnation, conventional dry impregnation and co-precipitation methods were employed for synthesis of Ni-Fe/ γ -Al₂O₃ catalyst. The catalysts were then characterised by XRD, TPR, Pulse Chemisorption and SEM-EDX analysis. Characterisation results obtained for Ni-Fe/ γ -Al₂O₃ catalyst were compared with Ni-Zn/ γ -Al₂O₃ catalysts and commercial nickel catalysts. The effects of different synthesis method on the characteristics of catalyst were investigated. Among the synthesised catalysts, those from co-precipitation method showed more desirable characteristics including higher metal loading, higher dispersions, smaller particle size and higher reducibility. Catalyst from co-precipitation method also

showed comparable characteristics with commercial catalysts which indicate a potential application in the hydrogenation process.

TABLE OF CONTENTS

DECLARATION	ii
APPROVAL FOR SUBMISSION	iii
ACKNOWLEDGEMENTS	vi
ABSTRACT	vii
TABLE OF CONTENTS	ix
LIST OF TABLES	xii
LIST OF FIGURES	xiv
LIST OF SYMBOLS / ABBREVIATIONS	xvii
LIST OF APPENDICES	xix

CHAPTER

1	INTRODUCTION	1
	1.1 Background	1
	1.2 Problem Statement	3
	1.2 Aims and Objectives	4
2	LITERATURE REVIEW	5
	2.1 Fats and Fatty Acids	5
	2.1.1 Saturated Fatty Acids	7
	2.1.2 Commercial Application of Saturated Fatty Acids	9
	2.2 Hydrogenation of Fatty Acids	10
	2.2.1 Reaction Mechanism	13
	2.2.2 Modification of Hydrogenation Process	15
	2.3 Catalysts for Hydrogenation of Fatty Acids	18

2.3.1	Nickel Catalyst	18
2.3.2	Palladium Catalyst	19
2.3.3	Iron Catalyst	20
2.3.4	Copper Catalyst and Ruthenium Catalyst	21
2.3.5	Bimetallic Catalyst in Alloy or Core-Shell Configurations	22
2.3.6	Raney Catalyst	23
2.4	Synthesis of Catalyst	24
2.4.1	Synthesis of Bulk Catalyst	24
2.4.2	Synthesis of Impregnated Catalyst	28
2.4.2	Heat Treatment	34
2.5	Characterisation of Catalyst	37
3	METHODOLOGY	39
3.1	Materials	39
3.2	Determination of Point-Zero Charge (PZC)	40
3.3	Determination of pH for Optimal Adsorption	41
3.4	Synthesis of Catalyst	42
3.4.1	Charge-Enhanced Dry Impregnation Method	42
3.4.2	Dry Impregnation Method	43
3.4.3	Co-Precipitation Method	43
3.5	Characterisation	45
3.5.1	X-ray Diffraction (XRD)	46
3.5.2	Temperature Programmed Reduction (TPR)	47
3.5.3	Pulse Chemisorption	48
3.5.4	Scanning Electron Microscopy with Electron Dispersive X-ray Spectroscopy (SEM-EDX)	49
4	RESULTS AND DISCUSSIONS	50
4.1	Determination of Point-Zero Charge (PZC)	50
4.2	Determination of pH for Optimal Adsorption	52
4.3	Observation from Synthesis of Catalyst	55
4.3.1	Charge-Enhanced Dry Impregnation Method	55

		xi	
	4.3.2	Dry Impregnation Method	56
	4.3.3	Co-Precipitation Method	57
4.4		Characterisation	58
	4.4.1	X-ray Diffraction (XRD)	58
	4.4.2	Temperature Programmed Reduction (TPR)	62
	4.4.3	Pulse Chemisorption	66
	4.4.4	Scanning Electron Microscopy with Electron Dispersive X-ray Spectroscopy (SEM-EDX)	69
5		CONCLUSION AND RECOMMENDATIONS	74
	5.1	Conclusion	74
	5.2	Recommendations	75
		REFERENCES	77
		APPENDICES	83

LIST OF TABLES

TABLE	TITLE	PAGE
2.1	Types of Saturated Fatty Acids	7
2.2	Composition of Fatty Acids in Coconut Oil and Palm Kernel Oil	8
2.3	Summary of Calcination and Reduction Conditions for Synthesis of Ni/ γ -Al ₂ O ₃ from Literatures	35
2.4	Formulas for Surface Properties Calculation	37
3.1	Summary of Characterisation Analyses on Each Sample	45
3.2	Conditioning Stages Prior to Pulse Chemisorption	48
4.1	Theoretical Calculation for Initial pH of Bulk Impregnating Solution	54
4.2	Optimum Reduction Temperature and Amount of Hydrogen Gas Adsorbed from TPR Analysis	62
4.3	Calculation Results for Pulse Chemisorption	65
4.4	EDX Elemental Composition Results of Ni-Fe Catalyst by Dry Impregnation Method	70
4.5	EDX Elemental Composition Results of Ni-Fe Catalyst by Co-Precipitation Method	71
4.6	SEM-EDX Results for Other Catalysts	72
A.1	Surface Loadings Calculation	83
E.1	Raw Data for PZC Determination	88
F.1	Adsorption Density for Nickel	90

F.2	Adsorption Density for Iron	90
H.1	Amount of Gas Adsorbed per gram of Metal	95
H.2	Metal Dispersion	95
H.3	Metal Surface Area	96
H.4	Metal Average Particle Size	96
I.1	Average Weight Percent of Metal Loadings	97

LIST OF FIGURES

FIGURE	TITLE	PAGE
1.1	Worldwide production volume of important oil sources in million tonnes	1
1.2	Industrial Oleochemistry Overview	2
2.1	Structural Formula of a Triglyceride with Fatty Acids of Varying Chain Length and Number of Double Bonds	5
2.2	Hydrolysis of Triglyceride with Base Catalyst	6
2.3	Alternating Melting Point of Saturated Acids	8
2.4	General Hydrogenation Scheme of C18 Fatty Acids	11
2.5	An Example of Industrial Hydrogenation Process	12
2.6	Reaction Mechanism of Hydrogenation	14
2.7	Two-step Hydrogenation Scheme	14
2.8	Effect of Varying Temperature on IV Reduction Rate	16
2.9	Effect of Process Conditions on Rate of Hydrogenation	17
2.10	Percent yield of alkenes in hydrogenation using amphiphilic polymer resin-stabilised iron nanoparticle catalyst	21
2.11	Hydrogenation with Iron Complex as Catalyst	21
2.12	Effects of concentration, pH and temperature on the solubility curve during precipitation	25

2.13	Schematic diagram of phases of alumina formed after thermal treatment	27
2.14	Illustration of Ion Adsorption on Solid Support with Adjusted pH	32
3.1	Summary of Dry Impregnation Method	43
3.2	Summary of Co-Precipitation Method	45
3.3	Shimadzu LabX XRD-6000 Machine	47
3.4	Thermo Scientific TPDRO 1100	48
3.5	Hitachi S-3400N SEM-EDX Machine	49
4.1	Equilibrium pH of γ -alumina at Different Surface Loading	51
4.2	Graph of Adsorption Density against Final pH for Nickel and Iron on γ -Alumina with SL= 600m ² /L	53
4.3	Catalyst synthesised by dry impregnation method before drying (left) and after calcination (right)	57
4.4	Catalyst synthesised by co-precipitation method before drying (left) and after calcination (right)	58
4.5	XRD Diffractogram for Ni-Fe/ γ -alumina by Dry Impregnation	59
4.6	XRD Diffractogram for Ni-Fe/ γ -alumina by Co-Precipitation	59
4.7	XRD Overlay diffractograms for (red) Ni-Fe by co-precipitation, (blue) Ni-Zn by co-precipitation, (pink) Ni-Fe by dry impregnation and (green) Ni-Zn by dry impregnation	61
4.8	TPR chromatogram of synthesised catalysts and commercial catalysts	64
4.9	TPR chromatogram of Ni-Fe catalysts by co-precipitation method (red line) and dry impregnation method (blue line)	65
4.10	SEM image of Ni-Fe catalyst by dry impregnation method (magnification x50)	69

4.11	SEM image of Ni-Fe catalyst by dry impregnation method (magnification x3000)	70
4.12	SEM image of Ni-Fe catalyst by co-precipitation method (magnification x6500)	71

LIST OF SYMBOLS / ABBREVIATIONS

m	mass of oxide support (g)
A	specific surface area of oxide support, (m^2)
V	volume of impregnating solution (L)
$C_{initial}$	initial concentration of impregnating solution ($\mu\text{mol/L}$)
C_{final}	final concentration of impregnating solution ($\mu\text{mol/L}$)
SL	surface loading of oxide support (m^2/L)
MW	molecular weight (g/mol)
Γ	adsorption density (nmol/m^2)
D	dispersion (%)
n	stoichiometry factor
M	metal loading (wt%)
$V_{adsorbed}$	volume of gas adsorbed ($\mu\text{mol/g}$)
$V_{gas,s.t.p.}$	volume of gas at standard temperature and pressure (dm^3/mol)
A_m	metal surface area (m^2)
N_A	Avogadro's number (atoms/mol)
a	cross sectional area of metal atom (m^2)
a_m	area of a metal atom on sample surface (m^2)
n_s	mean number of atoms on sample surface
V_m	volume occupied by an atom (m^3)
ρ	atomic mass density (g/m^3)
CEDI	charge enhanced dry impregnation
CP	co-precipitation
DI	dry impregnation
DP	deposition-precipitation
PZC	point zero charge

IV	iodine value
ICP-OES	inductively coupled plasma-optical emission spectrometer
SEM	scanning electron microscopy
EDX	electron dispersive x-ray spectroscopy
TPR	temperature programmed reduction
TPDRO	temperature programmed desorption/reduction/oxidation
XRD	x-ray diffraction
SL	surface loading

LIST OF APPENDICES

APPENDIX	TITLE	PAGE
A	Surface Loading Calculation	83
B	Calculation for Preparation of Catalyst by CEDI Method	84
C	Calculation for Preparation of Catalyst by Dry Impregnation Method	85
D	Calculation for Preparation of Catalyst by Co-Precipitation Method	86
E	Raw Data for PZC Determination in CEDI Method	88
F	Raw Data for Determination of pH for Optimal Adsorption in CEDI	89
G	Calculation of Theoretical Optimum pH for Adsorption in CEDI	91
H	Calculation on Pulse Chemisorption Results	92
I	Average Elemental Composition from SEM-EDX	97
J	Raw Data of Characterisation Analyses	98
K	Material Safety Data Sheet	104

CHAPTER 1

INTRODUCTION

1.1 Background

Fats and oils are among the most significant chemical compounds to mankind thanks to their functional versatility, flexibility and source abundance. They could be found naturally in plant extracts and animal tissues or synthetically produced. Major vegetable oil sources are palm oil and coconut oil in Asia, rapeseed and sunflower oil in Europe and soybean oil in America (Behr, 2008). Currently, Indonesia is the largest palm oil producer in the world and together with Malaysia, taking up more than 80% of the world's palm oil production (Suyenty, 2007).

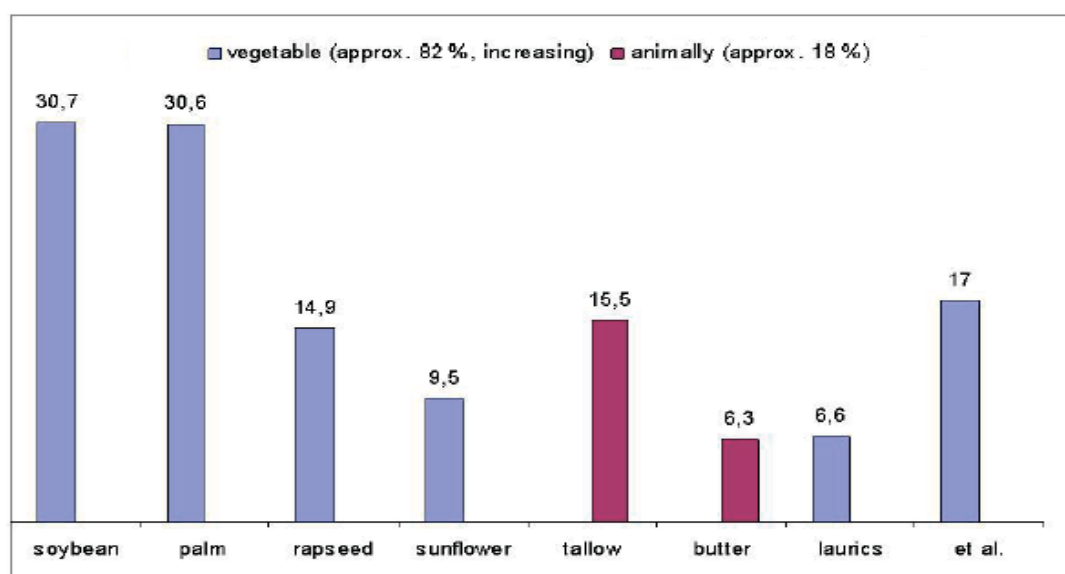


Figure 1.1: Worldwide production volume of important oil sources in million tonnes. (Behr, 2008)

Due to the abundance of plant-based oil sources, 80% of the world's production is from vegetable oils while the remaining is sourced from animal fats. From there, 86% of fats and oils produced are used for human and animal nutrition and approximately 14.2 million tonnes are utilized by the oleochemical industry (Anneken, 2000). Oleochemical literally refers to oil-based chemicals which are basic chemicals such as fatty acids, fatty alcohols, methyl esters and glycerols. These multifaceted oleochemicals are used either directly as raw materials or as basis for production of specialty chemicals as shown in Figure 1.2. With its advantage of non-toxicity and renewable source, oleochemicals are growing to be viable alternatives to crude oil derivatives.

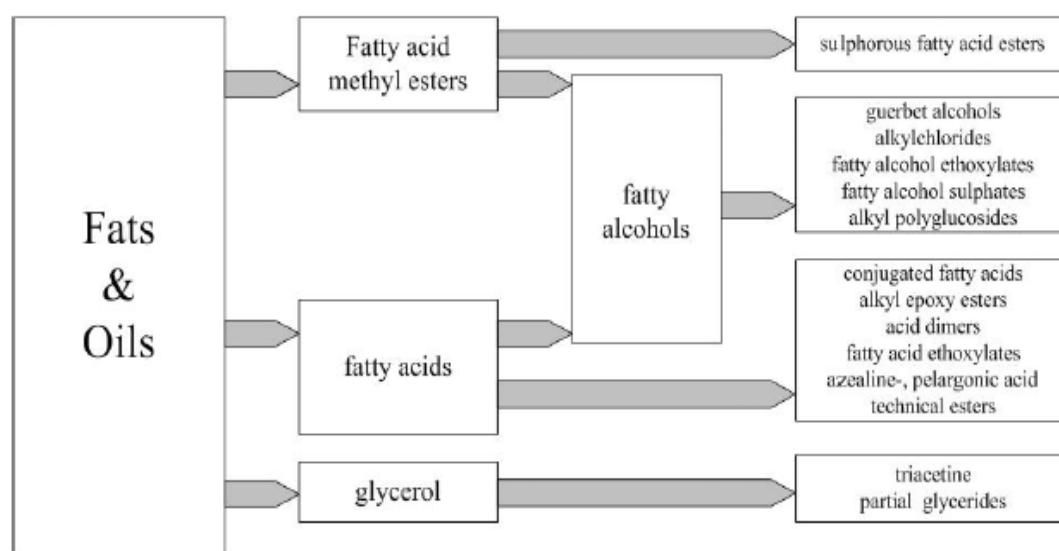


Figure 1.2: Industrial Oleochemistry Overview. (Behr, 2008)

In order to yield the useful oleochemicals, the raw triglyceride feedstock from either vegetable or animal source, has to be processed, refined and modified to suit the specific functions they are required to serve downstream. Commonly, the triglycerides would undergo hydrolysis to split the bulk oil molecules into fatty acids and glycerol. They are then distilled to remove odour and improve colour followed by fractional distillation to obtain individual fatty acids of varying chain length and characteristics. The separated fatty acids in particular the unsaturated fatty acids, would undergo modification processes such as hydrogenation to form oleochemicals with wide range of applications (Combs, 1985).

This project would focus on the full hydrogenation process which is carried out to convert unsaturated fatty acids to saturated fatty acids by adding hydrogen atoms to the fatty acid molecules. Through saturation, the fatty acids would be thermally more stable and contain higher amount of solid fats, enabling them to be used in more applications including lubricants, cosmetics and protective coatings. The importance of full hydrogenation is augmented in situations where unsaturated fatty acids are undesirable such as in metal stearates, rubber compounding and manufacture of candles and wax due to its low resistance to ambient oxidation and low heat stability (Suyenty, 2007).

1.2 Problem Statement

Although hydrogenation of fatty acids is a considerably well-developed and widely-applied process, concerns are projected on improving the performance of hydrogenation by cutting down processing time and cost as well as increasing the quality and consistency of product. This could be done by adjusting and optimising the reaction parameters such as temperature, pressure, agitation intensity and also by improvising the catalyst used in reaction.

Nickel catalyst is the most commonly used metal catalyst in the oleochemical industry due to its low cost and comparable activity. However, nickel catalyst is prone to deactivation by free fatty acids and other radicals in the oleochemical feedstock. Furthermore, the formation of nickel soap can lead to risk of contamination in the end-product. Further improvement of catalyst is therefore anticipated.

1.3 Aims and Objectives

The aim of this project is to synthesise and characterise Ni-Fe/ γ -Al₂O₃ bimetallic catalysts. The objectives are:

1. To synthesise Ni-Fe/ γ -Al₂O₃ catalyst employing charge-enhanced dry impregnation (CEDI), conventional dry impregnation and co-precipitation methods.
2. To characterise the prepared catalysts and commercial catalysts with XRD, TPR, pulse chemisorption and SEM-EDX.
3. To investigate the effect of different synthesis method on the characteristics of the catalyst.
4. To compare the characteristics of prepared Ni-Fe/ γ -Al₂O₃ catalysts with Ni-Zn/ γ -Al₂O₃ catalysts and commercial nickel catalysts.

CHAPTER 2

LITERATURE REVIEW

2.1 Fats and Fatty Acids

Fats are organic compounds made up of three fatty acid chains bonded to each of the hydroxyl (-OH) group of a glycerol, hence the name triglyceride indicates triesters of glycerol as illustrated in Figure 2.1. The fatty acid chains have varying length depending on the number of carbons. They are categorised into saturated and unsaturated fats judging by the presence of double bonds in their molecular structure. Saturated fats have no double bonds while unsaturated fats have at least one double bond. The extent of unsaturation is commonly represented by the iodine value (IV) which is denoted by the mass of iodine consumed for every 100g of oil in a standard test (Sonntag, 1982). Fats with higher IV value have higher degree of unsaturation. A molecule of fats could contain a mixture of fatty acid chains with varying length and number of double bonds.

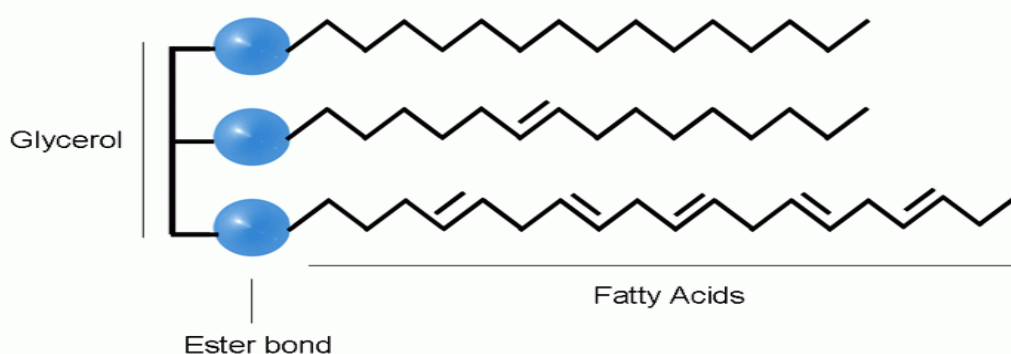


Figure 2.1: Structural Formula of a Triglyceride with Fatty Acids of Varying Chain Length and Number of Double Bonds. (Thiemann G., 2009)

In order to obtain fatty acids from triglycerides, the oil harvested from either plant or animal sources have to be hydrolysed. Hydrolysis could be carried out by addition of water while heating the fats at suitable temperatures which is called fat-splitting or with the help of acid catalyst, base catalyst or lipase enzyme to speed up the reaction. Base-catalysed hydrolysis is preferred when hydrolysing heat-sensitive fatty acids (Scrimgeour, 2005). Triglycerides are split into glycerol and fatty acids during hydrolysis as illustrated in Figure 2.2.

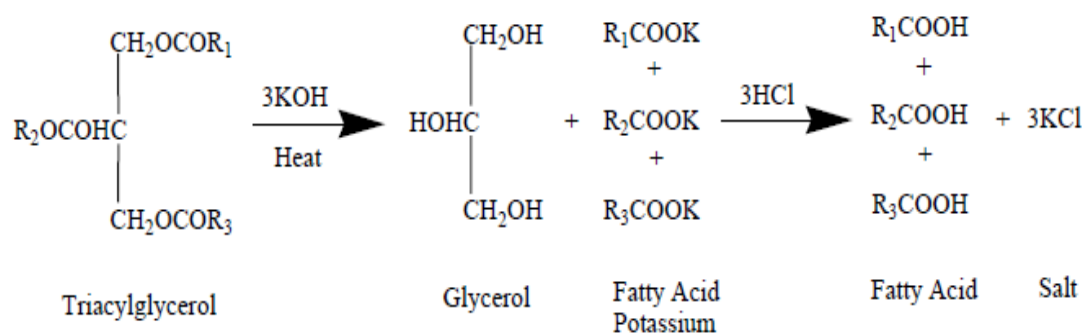


Figure 2.2: Hydrolysis of Triglyceride with Base Catalyst. (Salimon *et. al.*, 2011)

Hydrolysis of fats is commonly carried out by the Twitchell method, autoclave method or continuous method. Twitchell method relies on a catalyst to speed up the reaction while fats are heated with boiling water. In autoclave method, the reaction is sped up by intense heat. As for continuous method, the fats and water are continuously flowed counter-currently over a tower, also relying on heat to speed up the reaction. (Black, 1955) The crude fatty acids and glycerine produced have to be purified by distillation or solvent extraction and further processed into commercial products of pure fatty acids with purity up to 90 – 95% (Ruston, 1952).

2.1.1 Saturated Fatty Acids

Fatty acids with absence of double bonds are saturated and have very low IV value ($IV < 0.5$). Saturated fatty acids exist naturally in fats and oils or could be produced from full hydrogenation of other unsaturated fatty acids. There are various types of saturated fatty acids depending on their carbon chain length. Table 2.1 shows the different types of saturated acids with their respective chain length.

Table 2.1: Types of Saturated Fatty Acids. (Black, 1955)

Common Name	Number of Carbon Atoms	Geneva Name
Butyric	4	Butanoic
Caproic	6	Hexanoic
Caprylic	8	Octanoic
Capric	10	Decanoic
Lauric	12	Dodecanoic
Myristic	14	Tetradecanoic
Palmitic	16	Hexadecanoic
Stearic	18	Octadecanoic
Arachidic	20	Eicosanoic
Behenic	22	Docosanoic
Lignoceric	24	Tetracosanoic
Cerotic	26	Hexacosanoic

In warm climate, the major vegetable oil sources for fats are coconut oil, palm oil and olive oil. Meanwhile in temperate climate, the major sources are the annual plants including flax, soybean, cotton, peanut and castor bean which require cultivation (Black, 1955). Due to their high content of C_{12} to C_{14} fatty acids fractions which are highly sought after by the oleochemical industry, coconut oil and palm kernel oil are in good position as competitive oil sources as shown in Table 2.2.

Table 2.2: Composition of Fatty Acids in Coconut Oil and Palm Kernel Oil. (Gervajio, 2005)

Fatty Acid	Coconut Oil (%)	Palm Kernel Oil (%)
Caproic	0.2-0.8	0-1
Caprylic	6-9	3-5
Capric	6-10	3-5
Lauric	46-50	44-51
Myristic	17-19	15-17
Palmitic	8-10	7-10
Stearic	2-3	2-3
Oleic	5-7	12-19
Linoleic	1-2.5	1-2

At room temperature, those with shorter chain length of 4 to 10 carbon atoms exist as liquid while those with longer chain length present as wax-like solid. Generally, the melting point and boiling point of the saturated fatty acids increase with increasing chain length (Hoffman, 1989). However, odd-chain saturated fatty acids have lower melting point than their adjacent even-chain counterparts (Scrimgeour, 2005). This trend is depicted in Figure 2.3 below.

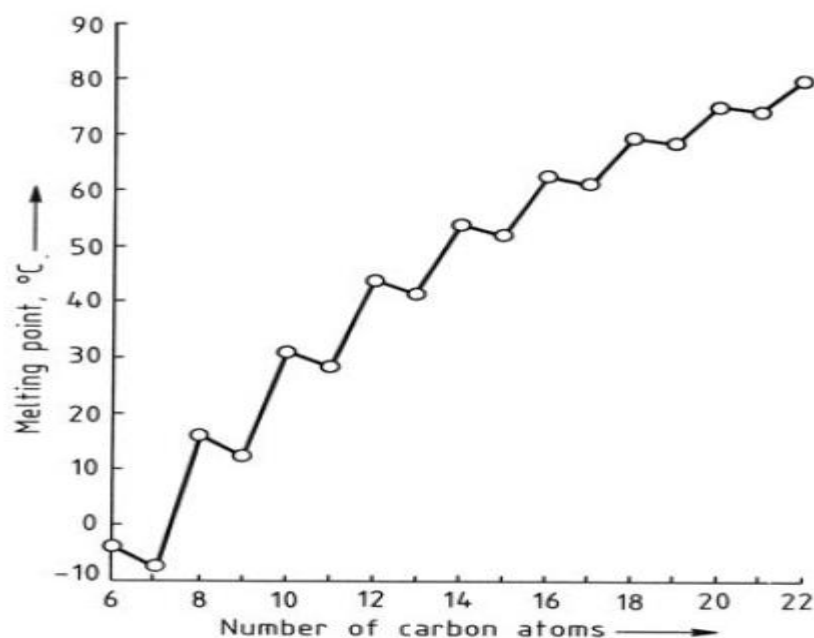


Figure 2.3: Alternating Melting Point of Saturated Acids. (Anneken, 2000)

Despite its saturated form, saturated fatty acids are not quite inert. Oxidation and halogenation process could be initiated by free radicals under high pressure and temperature where ionic mechanisms could easily cause substitution of halogen atoms in the chain. The fatty acid chains are also possible to rupture under exaggerated reaction condition (more than 300°C). Saturated fatty acids may also be decarboxylated by loss of carbon dioxide and form hydrocarbons under heating at high temperature in inert atmosphere (Hoffman, 1989).

2.1.2 Commercial Application of Saturated Fatty Acids

Over a century ago, candles were made from tallow which would release acrolein or tear-gas due to burning of its glycerol content. Chevreul's discovery that tallow could be split into glycerol and fatty acids has provided untold relief to countless people as the candles could then be made from fatty acids instead of tallow (Wittcoff, 1955). Fatty acids constitute a large part in the development and operation of oleochemical industry which bring about significant improvement to various consumer products impacting lives. Chemicals derived from natural oils are oleochemicals while those that are derived from petroleum feedstock (typically using ethylene as raw materials) are named petrochemicals.

Oleochemicals in particular fatty acids are involved in wide range of commercial uses such as rubber compounding, lubricating greases, engine oil additives, cleaning compounds and polishes, cosmetics, candles, textile chemicals and paper products. Among the saturated fatty acids, the ones with the most commercial importance are palmitic and stearic acids. Stearic acid, tallow or hydrogenated fatty acids are commonly used in rubber compounding to activate the accelerators and iron out the variations in curing speed. Almost every type of finished rubber products contains around 2% of fatty acids, making it one of the largest consumption of fatty acids (Ruston, 1952).

Besides that, fatty acids are also reacted with metals to form metallic soaps for various applications (Aylesworth, 1955). One such example is the gelling base of lubricating greases which is made from metallic fatty acids soap formed from the combination of saturated fatty acids with metals such as lithium, aluminium and sodium. Meanwhile, fatty acids derivatives such as chlorinated stearic acid are used as additives in engine oil as oil detergent and corrosion inhibitors. Moreover, tremendous amount of saturated fatty acids are used in manufacture of cosmetics and toiletries including shampoo, lotion and especially shaving cream. The white, creamy emulsion of the shaving cream could be obtained by saponification of stearic acid in conjunction with coconut fatty acid. The purity, colour and low IV of fatty acids are important to the manufacture of cosmetics in order to produce soft, large crystal for high quality product (Wittcoff, 1955). As for manufacture of candles, the white colour and rigidity are imparted by the use of stearic acid and hydrogenated fatty acids together with paraffin wax (Ruston, 1952).

2.2 Hydrogenation of Fatty Acids

Unsaturated fatty acids are hydrogenated in order to increase the melting point, solid fats content and oxidative stability while retaining their carboxyl functionality (Gutsche, 2008). Unsaturated fats tend to turn rancid due to oxidation when the reactive double bonds react with oxygen in the air. Hydrogenation helps improve their stability in air and during exposure to heat by reducing or eliminating the double bonds (Bartholomew *et. al.*, 2006). This enables them to be more viable for high temperature application. During hydrogenation, hydrogen atoms would be bonded to the double bonds available on the fatty acid chains hence reducing the number of double bonds. In addition, the fatty acids would also undergo *cis*- to *trans*-isomerisation (Veldsink J.W., 1997). The general hydrogenation scheme between C18 fatty acids of concern is illustrated in Figure 2.4.

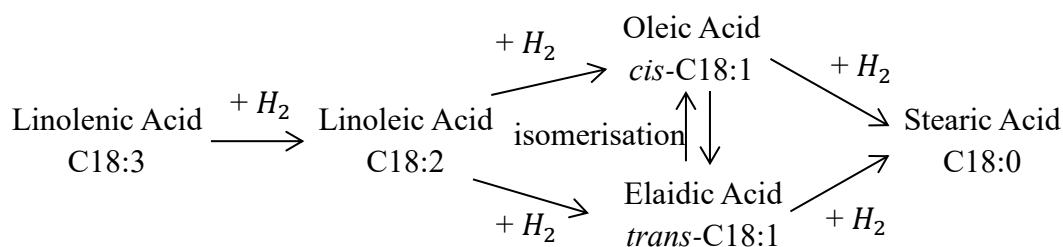


Figure 2.4: General Hydrogenation Scheme of C18 Fatty Acids. (Veldsink, 1997)

Hydrogenation of fatty acids is a three-phase process carried out by reacting hydrogen gas and fatty acids at elevated temperature and pressure with the presence of solid catalyst. Generally, industrial full hydrogenation is carried out by passing unsaturated fatty acids into a dryer followed by mixing with hydrogen gas and nickel catalyst slurry as shown in Figure 2.5. The reaction is then carried out at 25 atm and 453K to 523K (Suyenty, 2007). With reference to Hoffman (1989), the exothermic hydrogenation reaction has enthalpy of 0.92 - 0.95 kcal kg⁻¹ per iodine value unit or 27 - 28 kcal mol⁻¹ per double bond present. The heat emitted is sufficient to increase the temperature of hydrogenated mass by 1.9 - 2.1°C per iodine value unit saturated but due to the heat loss from the reactor walls, the net rise of temperature would be about 1.6 - 1.7°C per iodine value unit saturated.

Concurrently, Gutsche (2008) pointed that for the highest productivity, full hydrogenation is typically carried out with nickel catalyst at 130°C - 230°C and 2.5 MPa - 3.5 MPa in order to reduce nickel saponification and enhance hydrogen mass transfer. Besides that, the difficulties of filtering the colloidal nickel particles from the product after hydrogenation could be mitigated by adding 1 kg - 2 kg of inorganic filter aid per tonne of crude oil and circulated to form a primary filter cake. This was claimed to be able to achieve retention of 1 µm - 10 µm catalyst particles.

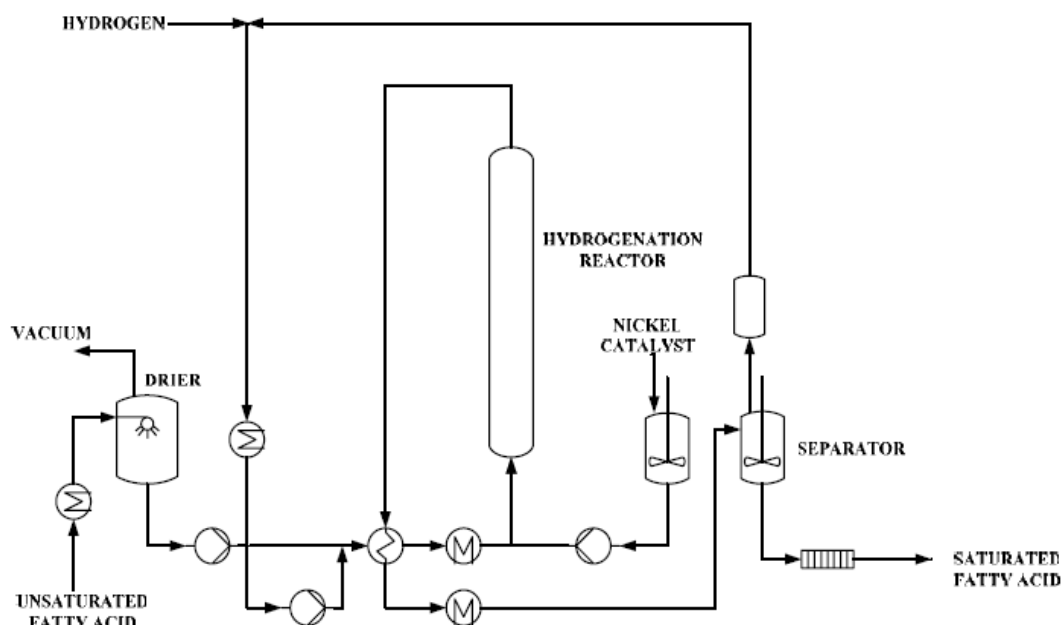


Figure 2.5: An Example of Industrial Hydrogenation Process. (Suyenty, 2007)

Hydrogenation could also be carried out batch-wise. According to Hoffman (1989), one third of the oil feed is first premixed with the fresh catalysts in this type of system. The remaining two third of oil is then added into the evacuated autoclave or reactor vessel followed by preheating and well-stirring. The previous oil-catalyst mixture is then added into the bulk of oil in the vessel and some hydrogen is vented off to purify the headspace. Further hydrogen gas addition may start at 120°C up to the prescribed reaction temperature. The exothermic character of the process has to be taken into account during heating by turning off the heat valves at 20°C below the set temperature.

Hydrogenation of fatty acids is prone to be confused with hydrogenation of fats (in triglycerides form). Other than having different feed materials, their process conditions also differ. According to Gutsche (2008), hydrogenation of fatty acids requires higher pressure compared to hydrogenation of triglycerides which needs pressure around 0.05 MPa - 0.5 MPa. The nickel catalyst consumption of hydrogenation of fatty acids is also higher at 500 ppm to 2500 ppm by weight in contrast with 100 ppm to 500 ppm by weight required in hydrogenation of triglycerides. Moreover, in hydrogenation of fatty acids, the process is started with pressurising at 100°C - 130°C to final temperature of 180°C - 240°C depending on the

initial IV. Meanwhile, for hydrogenation of triglycerides, a definite temperature has to be maintained by applying intensive cooling to the exothermic reaction.

In terms of storage and handling of fatty acids, impurities in the unsaturated fatty acids feed such as sulphur, bromine, phosphorus and nitrogen compound have to be kept below 1ppm to prevent catalyst poisoning. The fatty acids also have to be free from gummy materials, unsaponifiables and metallic impurities especially copper and iron which would affect the colour of the fatty acids and increase risk of turning rancid. Besides that, the materials used for construction of hydrogenation equipment also have to be corrosion resistance and able to prevent metallic contamination. Some common construction materials used are stainless steel type 316, aluminium, glass, rubber and acid-resistant tiles (Zinzalian, 1955). It is also important to provide a nitrogen atmosphere in the headspace of containers containing fatty acids to inhibit air oxidation and decolouration as well as prevent stratification.

2.2.1 Reaction Mechanism

According to Hoffman (1989) and Gutsche (2008), the hydrogenation reaction starts by dissociative chemisorption of hydrogen molecule (H-H) to active sites on nickel catalyst forming two polarised σ -bonded hydrogen on nickel (M-H) based on Polanyi-Horiuti mechanism. The carbon-carbon double bond also undergoes chemisorption at the catalyst active site by their π -system (C=C) forming temporary σ -bond (M-C). When in close neighbourhood or adjacent to each other, the σ -bonded hydrogen on nickel (M-H) would react stepwise with the σ -bonded carbon (M-C) first forming a half-hydrogenated intermediate. Subsequently, if the other σ -bonded carbon atom in the half-hydrogenated intermediate becomes free, it can accept another σ -bonded hydrogen atom in the neighbourhood and the double bond of the carbon chain becomes saturated. The saturated compound is then desorbed due to lower adsorption strength compared to its previous unsaturated state. The general scheme of this reaction mechanism is shown in Figure 2.6.

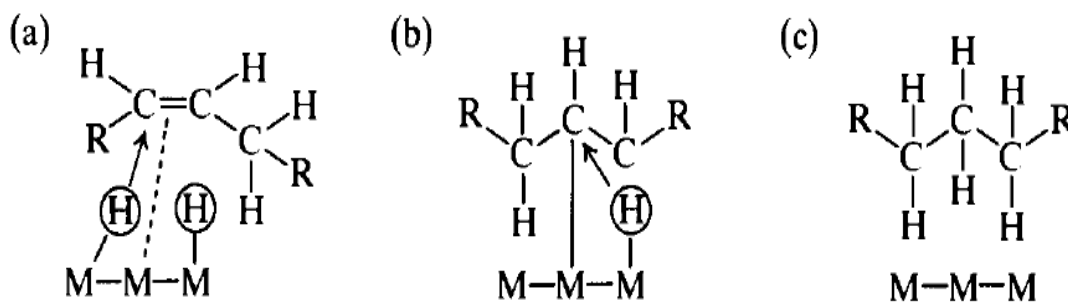


Figure 2.6: Reaction Mechanism of Hydrogenation. (a) π -complex (b) half-hydrogenated intermediate (c) saturated state. (Hoffman, 1989)

Furthermore, Scrimgeour (2005) explained that hydrogenation proceeds in two steps with semi-hydrogenated intermediate as shown in Figure 2.7. The first step is the reversible addition of one hydrogen atom. The semi-hydrogenated intermediate is unstable as it is able to generate double bond with altered position or geometry in which the process is termed as isomerisation. The addition of the second hydrogen in the second step is non-reversible and results in a saturated bond. It was also mentioned that for saturation of dienes, the first step is the rate-limiting step while for saturation of monoenes, the rate-limiting step is the second step. In addition, isomerisation of monoenes is favoured over saturation under low dissolved hydrogen concentrations, hence allowing control of product composition by change in hydrogen pressure, agitation and reaction time.

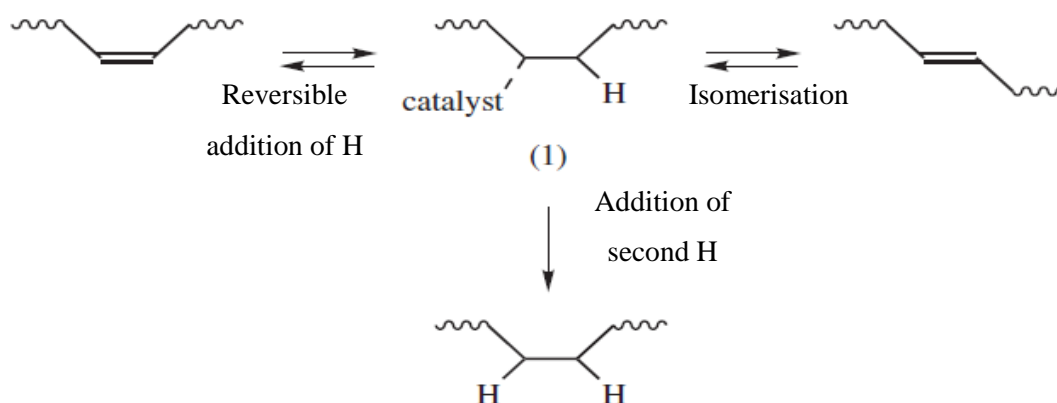


Figure 2.7: Two-step Hydrogenation Scheme. (Scrimgeour, 2005)

2.2.2 Modification of Hydrogenation Process

One of the main objectives of hydrogenation is to decrease the IV as fast and as low cost as possible in order to increase productivity and economic gain without compromising on product quality. In order to improve the performance of hydrogenation, various variables could be adjusted and modified including reactor design, process conditions, feedstock quality and catalyst design. Reactors designed for both hydrogenation of fatty acids and edible oils are essentially similar. However, reactors designed for hydrogenation of fatty acids have to be constructed from stainless steel and are required to withstand higher maximum pressure of 500psig or more. Meanwhile, reactors for hydrogenation of edible oils are usually designed for maximum pressure of 100psig (Hastert, 1979).

Modifications in terms of process conditions such as temperature, pressure and agitation speed are most often studied. Increments of reaction temperature and hydrogen pressure were found to increase rate of reduction of IV (Tike, 2006). However, the rise of temperature and pressure industrially to improve reaction performance are limited by the economic consideration of high energy cost and construction cost of more robust process vessels. In addition, although increasing the temperature greatly would increase rate of IV reduction, there would be diminished and negative effect if the optimal temperature range is exceeded as shown in Figure 2.8 (Hastert, 1979). Different fatty acids have varying optimal temperature for hydrogenation but they are generally in the range of 180 - 210°C.

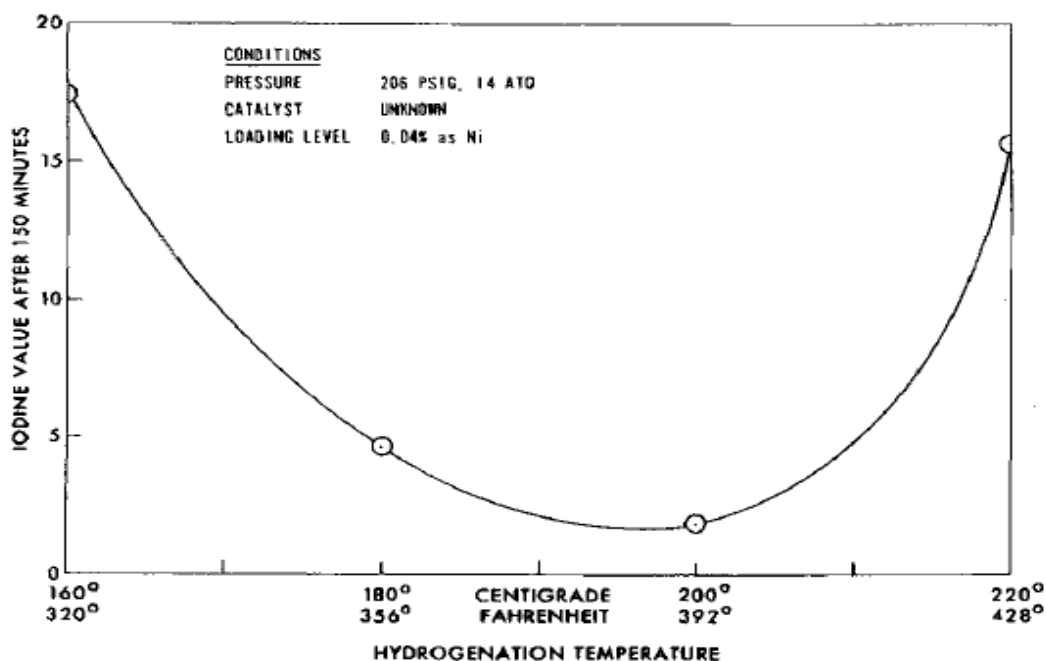


Figure 2.8: Effect of Varying Temperature on IV Reduction Rate. (Hastert, 1979)

The reacting fatty acids in the reactor has to be stirred or agitated in order to disperse the hydrogen gas into fine bubbles so that there are sufficient mass transfer and solubility of hydrogen gas in the liquid substrate. Agitation also enables the fine catalyst powders to be uniformly suspended in the liquid oil and the liquid substrate film layers around the catalyst particles are continuously renewed. The transport of hydrogen through the bulk liquid to the catalyst surface could be enhanced by increased mixing efficiency. Increasing the stirrer speed to improve mixing efficiency could avoid hydrogen starvation on the catalyst surface (Beers, 2007). It also helps in enhancing heat transfer in the reactor to achieve homogeneity of process conditions in the reactor (Gutsche, 2008). Increasing agitation speed increases the reaction rate and the maximum reaction rate is reached between 900-1000 rpm but this is again limited in the industry due to economic considerations (Hastert, 1979). In order to help enhance dispersion of hydrogen gas in the liquid, fresh hydrogen gas is introduced into the reactor by a sparging ring at the bottom of the reactor. Some of the gas would react with the liquid while some could not dissolve in time and rise to the reactor headspace. Thus the headspace gas must be vented out or recycled to prevent pressure build up.

Besides that, reduction rate of IV is faster at lower fatty acids concentration due to high catalyst/fatty acids ratio as more catalysts are available for reaction. The hydrogenation rate would also be profoundly increased by increasing the catalyst loading where the initial rate of reaction increases linearly with catalyst loading (Tike, 2006). To prevent the nickel catalyst from being deactivated by formation of soaps before reaction is completed, the catalysts are only added into reactor just before hydrogenation starts. Some also choose to hydrogenate the triglycerides before splitting to avoid deactivation of nickel catalyst due to reaction with free fatty acids (Hastert, 1979). The general effect of each process condition on the rate of hydrogenation is shown in Figure 2.9.

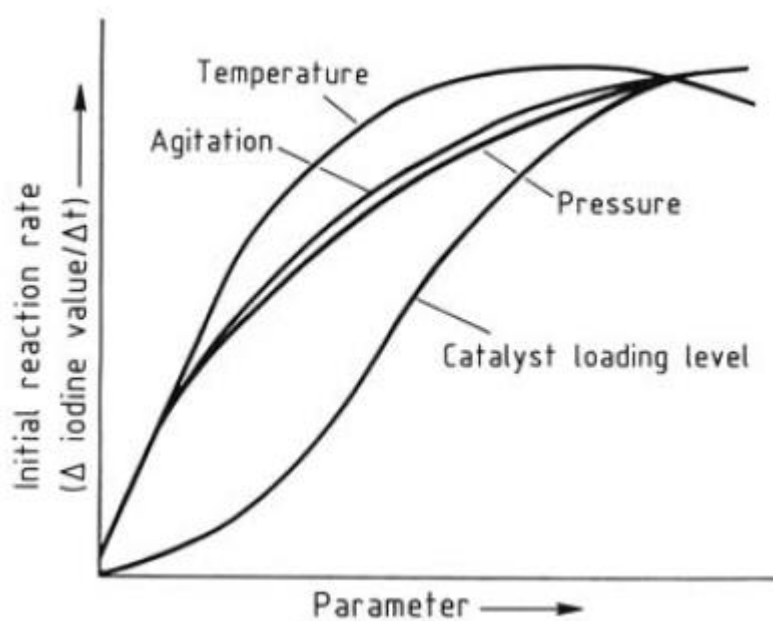


Figure 2.9: Effect of Process Conditions on Rate of Hydrogenation. (Anneken, 2000)

For hydrogenation of feedstock with very high IV, two-stage hydrogenation may be necessary by adding more catalyst at the second stage. Long residence time in high temperatures should also be avoided as it would cause increased formation of nickel soap (Hoffman, 1989). Therefore, in order to improve overall batch hydrogenation economics, the batch reaction cycle time could be reduced and feedstock raffination should be extended so that risk of catalyst poisoning is lowered (Gutsche, 2008).

2.3 Catalysts for Hydrogenation of Fatty Acids

Various types of catalyst for hydrogenation (not limited to fatty acids) are explored in the following sections.

2.3.1 Nickel Catalyst

The most commonly used catalyst for full hydrogenation of fatty acids is 20-25 wt% nickel catalyst supported on diatomaceous earth made by dry reduction method. This type of catalyst is favoured in the industry because of its lower cost, versatility and almost similar catalytic performance compared to precious metals when operated at high temperatures.

There are also other types of nickel catalyst where the active nickel metals are supported on alumina which takes up about 10-15 wt% of the catalyst. The alumina support helps to increase the active sites dispersion and creates larger mean pore size diameter resulting in better accessibility to the whole nickel surface area (Gutsche 2008).

Generally, nickel needs high operation temperature as it is not active below 120°C (Jang *et. al.*, 2005). Nickel also tends to react with fatty acids to form nickel soap which would deposit on catalyst and decrease its activity (Henderson, 1992). Concurrently, water is also a powerful nickel catalyst deactivator, thus calling for the need to remove water from the fatty acids feedstock before reaction (Tike, 2006).

Due to its pyrophoricity, nickel catalyst is usually coated with fully hardened fatty acids with melting point of 50 - 60°C to avoid air oxidation (Hastert 1979). The fat coating is also reported to provide good resistance against poison substrates such as sulphur compounds, phospholipids and trace metals (Gutsche, 2008).

2.3.2 Palladium Catalyst

Palladium was proposed as an alternative to nickel catalyst mainly due to its ability to remain active at low temperature and pressure which would help to reduce cost in energy and vessel construction. Palladium catalyst on silica support was compared with commercial nickel catalyst in a research by Belkacemi (2009). It was found that palladium catalyst was more selective and needed lower metal loading to achieve similar activity with the commercial nickel catalyst. Palladium catalyst was also found to be active even at low temperature of 80°C and low pressure of 3.6 atm at which nickel catalyst did not exhibit any activity. The activation energy needed by palladium catalyst to hydrogenate oil is less than that of nickel catalyst, hence enabling palladium to be active at lower temperature condition.

Synthesis of palladium catalyst supported on magnesium oxide was reviewed by Toebe (2000). It was pointed out that palladium precursors that could be used include palladium nitrate in water or palladium chloride in diluted chloric acid. However, it was found that catalyst prepared using palladium chloride has higher ion-concentration on the support surface than the one prepared by using palladium nitrate as precursor.




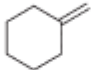
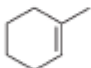
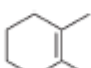
In another research by Savchenko (1999), palladium catalyst on alumina support was proposed over nickel catalyst. Nickel was said to contaminate the product by reacting with the free fatty acids to form fat-soluble salt. Similar to Belkacemi, Savchenko also found that palladium catalyst could be used at lower temperature than nickel catalyst at 150 °C. As palladium is more costly, the economics could be improved by reducing the amount of palladium used as it was found that when the amount of palladium was increased by 10 times the rate of reaction was only increased by 2 times. It was proposed that only 1-2g palladium catalyst is needed for every tonne of feedstock with the condition that the fatty acid feedstock has to be cleaned in the initial preparation stage as palladium catalyst is prone to poisoning especially by sulphur. Palladium catalyst could also be regenerated many times to reduce the consumption of fresh palladium metal. In addition, Savchenko also discovered that the hydrogenation reaction mostly occurred at the catalyst surface shell due to transport limitation.

2.3.3 Iron Catalyst

Iron catalyst is another transition metal catalyst that is used in the industry for hydrogenation. It is a predominant commercial catalyst for Fisher-Tropsch process. It is also applied in the hydrogenation of carbon dioxide to form useful hydrocarbons via reversed water-gas shift followed by Fisher-Tropsch process as it shows remarkable performance in both processes (Lee, 1989).

Currently, unsupported iron catalysts are used with fewer studies on supported iron catalyst probably due to its very low cost (Jung, 1982). Its wide usage is also contributed by its abundance where iron is the second most abundant metal in Earth's crust as well as its low toxicity compared to other metal catalysts (Michaelis, 2008). Enhanced by its facile change in oxidation state and distinct Lewis acid character, iron catalyst in principle allows a broad range of synthetic transformations including hydrogenation, oxidations, additions, substitution and isomerisation (Enthaler, 2008).

Furthermore, based on findings by Hudson (2013), highly efficient catalytic hydrogenation could be achieved with the use of amphiphilic polymer resin-stabilised iron(0) nanoparticle catalyst in ethanol or water in a flow reactor. Through this, alkenes, alkynes, aromatic imines and aldehydes could be hydrogenated nearly quantitatively. Figure 2.10 shows the yield for different alkenes hydrogenated with the iron nanoparticles. The accessible surface iron is responsible for catalytic activity while the iron nanoparticle catalyst is stabilised and protected by amphiphilic polymer resin support which enables long term stability and high catalytic activity. With the amphiphilic polymer resin, iron remains zero valent state despite exposure to water and oxygen in the flow reactor. The resin support is also able to extract organic substrates from aqueous phase resulting in higher concentration of substrates near the catalyst surface thus speeding up reaction. This amphiphilic polymer resin-stabilised iron nanoparticle catalyst is robust, cheap and environmentally friendly novel technology for chemoselective hydrogenation. Due to its robustness in presence of water, it is deemed as a realistic competitor to platinum catalyst for application in hydrogenation.

Entry	Substrate	Yield (%)
1		90
2		87
3		83
4		14
5		6
6		Trace

^a Reaction conditions: 40 bar H₂, 100 °C, 0.5 mL min⁻¹, 0.05 M substrate in EtOH (residence time 116 seconds).

Figure 2.10: Percent yield of alkenes in hydrogenation using amphiphilic polymer resin-stabilised iron nanoparticle catalyst. (Hudson, 2013)

Besides that, iron complex can catalyse hydrogenation of simple alkenes with higher turnover frequency than ruthenium or iridium catalyst (Michaelis, 2008). The iron complex under discussion was low-valent bis(imino)pyridine iron complex which could be synthesised by reduction of dihalogen complex with sodium amalgam under nitrogen atmosphere (Enthaler, 2008). Figure 2.11 shows reaction scheme and conditions of hydrogenation with the use of iron complex.

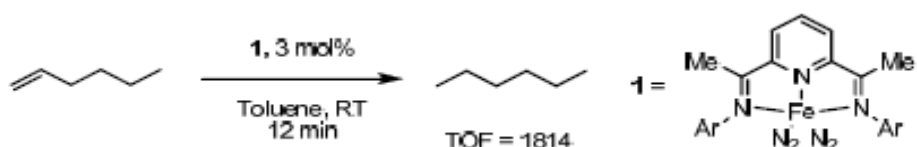


Figure 2.11: Hydrogenation with Iron Complex as Catalyst. (Michaelis, 2008)

2.3.4 Copper Catalyst and Ruthenium Catalyst

Copper catalyst could also be used in hydrogenation of fatty acids. It has high linolenic selectivity and is more effective in stopping the reaction at monoenoic acid

level. This is an advantage if applied in edible oil industry where partial saturation of fatty acids is required with low trans-fats and saturated fats formation. Copper catalyst is less active than nickel catalyst in hydrogenation, resulting in about 5-10 times more copper catalysts needed per batch of reaction compared to nickel catalyst (Hoffman, 1989)

Besides that, ruthenium catalyst is also an alternative studied for hydrogenation of fatty acids. It has been known to be a good catalyst for hydrogenation of organic substrate in the presence of water. Ruthenium catalyst is tolerant to water content unlike nickel catalyst thus dehydration of feedstock beforehand is not needed. This could help in reduction of operating cost and process intensification as the process cycle is shorter. Ruthenium is more costly than nickel but is less expensive than platinum and palladium (Tike, 2006).

2.3.5 Bimetallic Catalyst in Alloy or Core-Shell Configurations

The use of dual metals in the catalyst alters the electronic structure of the active phases which helps to enhance its catalytic performance (Hwang, 2013). Bimetallic catalyst commonly involves combination between noble metals or between noble metals and non-noble metals. This would reduce the noble metals loading which could be very costly in the catalyst.

Bimetallic catalyst could be synthesised in alloy or core-shell configurations. According to research done by Viet Long (2011) on platinum and palladium nanoparticles bimetallic catalyst on carbon support, the core-shell configuration catalyst showed better catalytic activity than the alloy despite the fact that the core-shell configuration had larger pore size than the alloy. It was explained that this was due to synergistic effect whereby “the nanocore gave a ligand effect on the nanoshell element because the surface atoms of the nanoshell are coordinated to the nanocore in the catalytic reaction”. Viet Long also pointed out that the core-shell structure could better suppress adsorption of poisonous species as it modified the electronic band structure for better surface adsorption of the reactants.

The advantages of core-shell configuration were also mentioned in a research on platinum and palladium bimetallic catalyst by Hwang (2013). It was deduced that high platinum utilization could be achieved due to interposition with the non-noble metal core thus increasing the economics of the costly noble metal. The structure was further stabilized by the alteration of platinum electronic structure which enhanced the interfacial bonding between the core and shell.

Besides that, Persson *et. al.* (2006) found that the incorporation of platinum into palladium catalyst could increase catalytic activity and the platinum would also improve stability of palladium during reaction. Bimetallic catalyst shows distinct electronic and chemical structure from their parent metal hence providing opportunity to obtain new catalyst with higher selectivity, activity and stability by using the same types of metal (Weiting Yu *et. al.*, 2012).

2.3.6 Raney Catalyst

Raney catalyst could also be applied in hydrogenation of organic substrate including those with C=C groups, oxygen containing groups and reducible nitrogen containing groups. Based on Harper (2000), Raney catalyst is a catalyst comprising of iron, cobalt and a third metal which is commonly selected from nickel, rhodium, ruthenium, palladium, platinum, osmium and iridium. Usually, nickel is preferred as the third metal component with the preferred Raney catalyst concentration of 50wt% iron, 15wt% cobalt and 2wt% nickel.

The combination of iron and cobalt gives a stable catalyst while the combination of iron and nickel results in a desirable active catalyst but with short lifetime due to rapid deactivation. Hence, Raney catalyst which takes advantage of the characteristics of the metal combinations could achieve good stability and high activity. Raney catalyst could be used in hydrogenation of unsaturated organic compounds at 50 - 2000 psig or 13.78 MPa and 25 - 150°C. It is particularly effective in hydrogenation of nitriles.

2.4 Synthesis of Catalysts

Catalyst synthesis is very diverse and each could follow a distinct route. Generally, three fundamental stages are involved according to Haber *et. al.* (1995):

1. Preparation of precursory solids associating all the components required.
2. Processing of the solids to obtain catalyst precursor, most commonly by heat treatment.
3. Activation of precursors to get the active catalyst.

The synthesis of catalyst should be able to result in catalysts with high surface area, porosity, high mechanical strength and thermal stability.

Catalysts could be classified based on their synthesising mechanism where bulk catalyst and impregnated catalyst are the two major types according to review done by Campanati (2003). Bulk catalyst has its active phase and/or support generated as new solid phases while impregnated catalyst has its active phases fixed on a pre-existing solid support. The following sections describe the two synthesising mechanisms in greater detail.

2.4.1 Synthesis of Bulk Catalyst

Bulk catalysts are synthesised through precipitation of solid from liquid solution containing precursors. The three steps involved in precipitation of crystalline solid are supersaturation, nucleation and growth (Serpell, 2011). In supersaturation stage, the system is unstable and any perturbation would result in precipitation. Supersaturation could be achieved by physical means and chemical means. Physical means involve cooling down of reaction mixture or evaporation of solvent. Chemical means it is done by adding precipitation agent which changes the pH and causes condensation of precursors to form hydroxides or oxides. According to Lok (2009), when precipitating nickel nitrate with sodium carbonate, higher pH leads to higher degree of completion. The precipitating agent could also introduce additional ions so that the solubility of certain precipitate is exceeded. The effects of increasing

concentration, pH and temperature on solubility of the precursors which results in precipitation are shown in Figure 2.12.

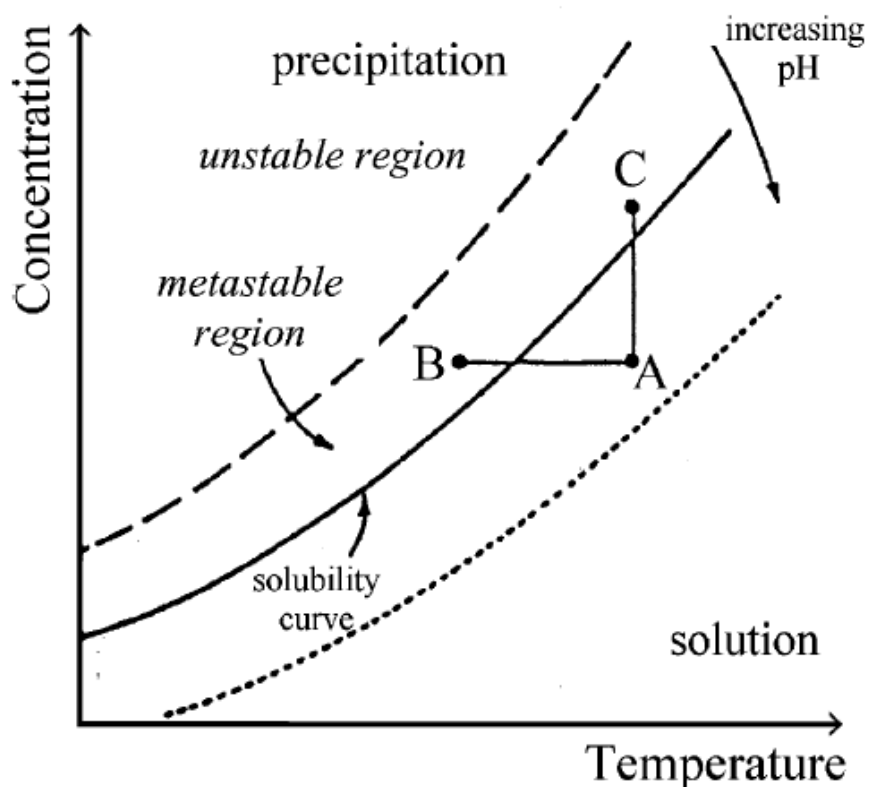


Figure 2.12: Effects of concentration, pH and temperature on the solubility curve during precipitation. (Campanati, 2003)

Supersaturation state is the most important factor in determining the morphology, texture and structure of the precipitated catalyst. However, supersaturation could only be maintained for a short time and within limited volume of solution due to the nature of the system favouring decreased supersaturation by consumption of reagents for nucleation (Schwarz, 1995). Nucleus, which is the smallest elementary particles of the new solid phase is formed during nucleation and further propagates in the growth stage. Nucleus formation and precipitation would begin if the precursor concentration exceeds the critical threshold concentration of the nucleation curve. If the precursor concentration falls below the critical level due to consumption of precursors by nucleation or growth, only particle growth of existing particles would prevail. (Ertl *et. al.*, 1999)

Co-precipitation is also possible to produce bimetallic catalyst or active phase with support by intimate mixing of the liquid solutions containing the constituent components. This method creates very small and intimately mixed crystallites to produce catalyst with good dispersion of metal phase. During co-precipitation, if one component is more soluble than the other, sequential precipitation would occur and result in less intimate mixing of components due to presence of concentration gradient in the product. This could be avoided by carrying out precipitation at higher supersaturation to exceed solubility of both components simultaneously. It is preferred to operate at constant pH with simultaneous addition of reactants so as to minimise the concentration gradient in the precipitating vessel. (Lok, 2009) In order to achieve more homogeneous product, mixed metal solution is added to existing precipitating agent so that the precipitating agent would always present in large excess hence preventing metal with lower solubility from precipitating first. Catalyst with smaller particle size and higher surface area could also be achieved by precipitating at higher concentration level which enhances the nucleation rate. (Ertl *et. al.*, 1999)

According to Ertl *et al.* (1999), precipitation of active alumina support is more complex due to the rich chemistry of alumina. Phases present in raw material and thermal treatment at different temperature would result in alumina of different phases. The synthesis pathway for various phases of alumina is illustrated in Figure 2.4 below. In order to yield γ -alumina, aluminium salt solution is neutralised with bases at pH 7 - 12 to precipitate out aluminium hydroxides. If it is carried out at high temperature and pH, bayerite would form while at lower pH, pseudoboehmite and boehmite would be formed. Heating of the aluminium hydroxide to different temperature according to the schematic pathway in Figure 2.13 would lead to formation of various phases of alumina. For γ -alumina, it is heated to between 773 K and 1173 K. In Figure 2.2, pathway (a) is favoured by pressure exceeding 1 bar, in moist air with heating rate larger than 1 K min^{-1} for particle size larger than $100 \text{ }\mu\text{m}$ whereas pathway (b) is favoured by pressure below 1 bar, in dry air with heating rate lower than 1 K min^{-1} for particle size smaller than $10 \text{ }\mu\text{m}$.

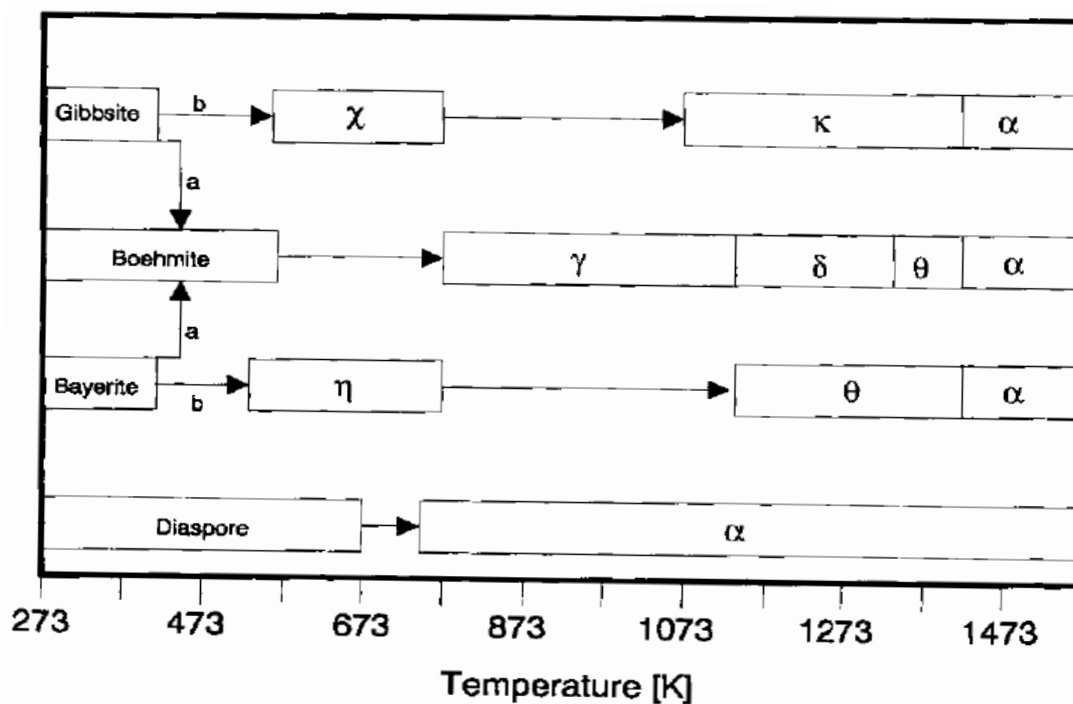


Figure 2.13: Schematic diagram of phases of alumina formed after thermal treatment. (Ertl *et. al.*, 1999)

Synthesis of nickel catalyst on alumina support for selective hydrogenation of fats and oils was demonstrated in a patent by Broecker *et. al.* (1973). A metal precursor solution containing nickel nitrate hexahydrate and aluminium nitrate nonahydrate dissolved in water was prepared as Solution 1 to yield the metal precursor with the formula $\text{Ni}_6\text{Al}_2(\text{OH})_{16}\text{CO}_3 \cdot 4\text{H}_2\text{O}$. Similarly, Solution 2 which contained sodium carbonate was also prepared. Both of the solutions are prepared at molar concentration of 2M. Adequate amount of water was also added into the precipitating vessel and all the solutions were heated up to 80°C. It was reported that Solution 1 was added first to the vessel until pH 5 was reached. This was followed by simultaneous addition of both Solution 1 and 2 slowly to maintain the pH between 4.5 to 5.5. When Solution 1 has all been added, Solution 2 was also finished into the vessel to give a pH of 6.5. The slurry was then stirred at 80°C for another 15 minutes before it was filtered and washed until no more nitrates could be detected in the filtrate. The precipitates were dried in oven at 110°C and calcined at 350°C for 20 hours followed by reduction by hydrogen for 20 hours at 400°C to 470°C.

On a separate note, washing of the precipitates is also a vital step. Thorough washing of the precipitates is required in order to remove the metal nitrates and other water soluble compounds on the precipitate. According to Johannes *et. al.* (2011), for every 2 L of impregnating solution employed in co-precipitation of catalyst, the precipitates have to be washed with approximately 30 L of water. The large volume of water used for washing is to ensure that metal nitrate salt is dissolved and removed before subsequent heat treatment as these water-soluble salts are unlikely to be properly removed during heat treatment.

2.4.2 Synthesis of Impregnated Catalyst

Impregnated catalysts are synthesised by wetting pre-existing or pre-formed support with solution or slurry with active phase precursor. Impregnation, ion-exchange, adsorption and deposition-precipitation are the four common techniques in producing impregnated catalysts (Campanati, 2003).

a) Impregnation

In impregnation, a certain volume of solution containing the active phase precursor is made to be in contact with the solid support. The volume of impregnating solution used further differentiates it into two methods which are the wet impregnation and incipient wetness impregnation or dry impregnation (DI). Wet impregnation uses an excess of impregnating solution but the uptake of impregnating solution by the support is slow as the transport of solution into the pores is governed by diffusion. Meanwhile, for incipient wetness impregnation or dry impregnation, the volume of solution used is equal or slightly less than the pore volume of the support. Due to the limited impregnating solution in contact with the dry support, impregnation is carried out by capillary action hence enabling faster uptake of impregnating solution by the support. However, during subsequent drying and heat treatment, the capillary force also leads to rapid transport of impregnating solution to

external surface of the pellets followed by deposition at the external edges, resulting in egg-shell like distribution of active phase. (Geus, 2007) Concurrently, repeated applications of the solution to the support are necessary and the maximum loading of the active phase to the support is limited by the solubility of the precursor in the solution.

Dry impregnation method was used by Huang and Schwarz (1987) in their synthesis of alumina supported nickel catalyst. It was pointed out that the amount of metal deposited was controlled by the concentration of metal in the impregnation solution used. Huang and Schwarz used 2 g of gamma-alumina $\gamma - Al_2O_3$ with 5 cc of nickel nitrate hexahydrate as electrolyte. The pH of the solution was adjusted to the range of 1 to 5 by using nitric acid. The suspension was constantly shaken and allowed to dry completely. The solid samples were then dried at room temperature for 24 hours. It was found that at the same loading, the specific surface area and dispersion decreased with increasing pH. However, catalyst with loading of 0.9 wt% impregnated at pH 5 could achieve similar dispersion with catalyst with loading of 2.9 wt% impregnated at pH 1.

In another research by Batholomew and Farrauto (1976), alumina supported nickel catalyst was prepared by the dry impregnation method. The DI method was carried out by using pure nickel nitrate hexahydrate with γ -alumina. The samples were then dried in air at 80°C to 100°C. It was found that calcination at 400°C or 1 hour is detrimental to the catalyst, causing reduction in surface area and dispersion. Hence it was suggested that the calcination has to be above 600 °C. It was subsequently reduced in hydrogen gas with space velocity of 1500-200 hour⁻¹ at heating rate of 5°C/min to reach 230°C and held at 230°C for 1 hour. This was followed by heating slowly to 480°C and hold for at least 10 hours. The slow heating during reduction was required in order to prevent exothermic temperature that will badly sinter the catalyst.

Besides that, Epinosa *et. al.* (2008) also employed dry impregnation method in synthesising Ni/ γ -Al₂O₃ catalyst with 3 wt% nickel. Beforehand, the alumina pellets were calcined at 450°C for 8 hours and kept at 120°C until use. The volume of

impregnating solution was equal to the support pore volume plus 10%. The solution was added dropwise to the pellets and the pellets were shaken for 2 minutes for even distribution of solution. The 10% excess solution was removed and the impregnated pellets were kept for 2 hours in a closed vessel and subsequently dried in preheated oven with static air at 100°C for 8 hours.

On the other hand, Montes (1984) researched in the synthesis of silica supported nickel catalyst by dry impregnation (DI) and deposition-precipitation (DP) methods. It was found that DP method results in stronger interaction between metal precursor and the support while DI method yielded catalyst with weak interaction between the precursor and support leading to sintering. In the DI method, the catalyst was prepared by adding 42.8 g of nickel nitrate hexahydrate $\text{Ni}(\text{NO}_3)_2 \cdot 6\text{H}_2\text{O}$ to 79.2 ml of water with 99 g of silica support SiO_2 . The suspension was constantly stirred and the solid samples were then dried at 120°C for 16 hours under vacuum.

b) Ion-exchange and Ion Adsorption

For ion-exchange, the ions on the surface of support are replaced by ions from the solution with active phase precursor. This is done by plunging the support into an excess volume of solution to enable ions from the solution to gradually penetrate into the pores of the support while the ions from the support pass into the solution until equilibrium is reached. Meanwhile, the adsorption method is similar to the ion-exchange method whereby ionic species from the solution are attracted by the charged sites on the support electrostatically.

c) Deposition Precipitation (DP)

In deposition-precipitation, the two steps involved are precipitation from bulk solution and interaction with the support surface. Precursors of active phase in powder form are used to form slurries with sufficient concentration of precursors to

achieve the desired loading. Solid supports are then suspended in the precursor slurry. Precipitation is then caused by gradually adding alkali solution and made to deposit on the solid support surface evenly. Thoroughly stirring is a must to avoid high local concentration and precipitation in the solution instead of on the support surface. Hydrolysis of urea could be used as the source of hydroxide ions instead of conventional alkali for even deposition of precipitation on the support as urea dissolves in water and decomposes slowly upon heating to give uniform concentration of hydroxide ions.

In a review by Louis (1997), the example of nickel supported on silicon was given for the deposition-precipitation method. It was done by first suspending solid silicon support in solution containing nickel nitrate and urea at room temperature. Nitric acid was also added to help tracking the pH changes. The solution was stirred while being heated up to 90 °C where pH gradually increased and precipitation occurred on the support surface. The sudden nucleation of nickel precipitate on the support caused sudden drop in pH due to hydroxide ion consumption. The precipitation then proceeded at lower pH due to establishment of equilibrium between formation of hydroxide ions from urea hydrolysis and consumption of hydroxide ions for precipitation. It was found that the nickel loading increased with deposition-precipitation (DP) time but over long DP time, the supported active phase became ill-crystallized and hard to be characterized. High nickel loading (>20wt%), narrow size distribution of metal particles and high resistance towards sintering could be achieved by this method.

Another review based on findings by Lok (2000, 2004) gave the example of deposition-precipitation by ammonia evaporation. The method involved alumina powder in aqueous solution containing ammonia and nickel ammine. The initial pH was high (pH 9 to 11) due to presence of ammonia and the solution was heated to more than 70°C. Upon heating, the ammonia evaporated and the pH dropped while precipitation occurred. Meanwhile, in the DP method conducted by Montes (1984), 81.4 g of $\text{Ni}(\text{NO}_3)_2 \cdot 6\text{H}_2\text{O}$ and 80 g of silica support was added to 2 L of distilled water. Nitric acid HNO_3 was also added to adjust pH to 3.5. The suspension was then heated slowly to 90°C and 50.4 g of urea is gradually added. The reaction was run for 6 hours and the filtrate was then washed with distilled water at 90°C followed by

drying at 120°C for 16 hours. The final samples were calcined in air at 450°C for 16 hours and subsequently reduced by H₂ flowing at 190 ml/min per gram of catalyst at 500°C with heating rate of 8°C/min for 16 hours.

d) Charge Enhanced Dry Impregnation (CEDI)

Zhu *et. al.* (2013) proposed an improved synthesis method named Charge Enhanced Dry Impregnation (CEDI) as a combination of ion-adsorption and dry impregnation method. CEDI was basically developed to overcome the shortcoming of dry impregnation where there was lack of interaction between metal precursors and the support, resulting in vulnerability to sintering and poor distribution of metal phase. Zhu *et. al.* found that the support surface could electrostatically adsorb precursors of opposite charge if the support surface is protonated below its Point Zero Charge (PZC) or deprotonated above its PZC sufficiently. It is important to note that PZC is the pH at which the substance is neutrally charged. This ion adsorption mechanism is illustrated in Figure 2.14 whereby when the pH of solid support is below its PZC, the hydroxyl group would be protonated and metal complex of negative charge would be attracted and adsorb on it. On the other hand, when the pH is above its PZC, the hydroxyl group would be deprotonated and metal complex of positive charge would adsorb on it.

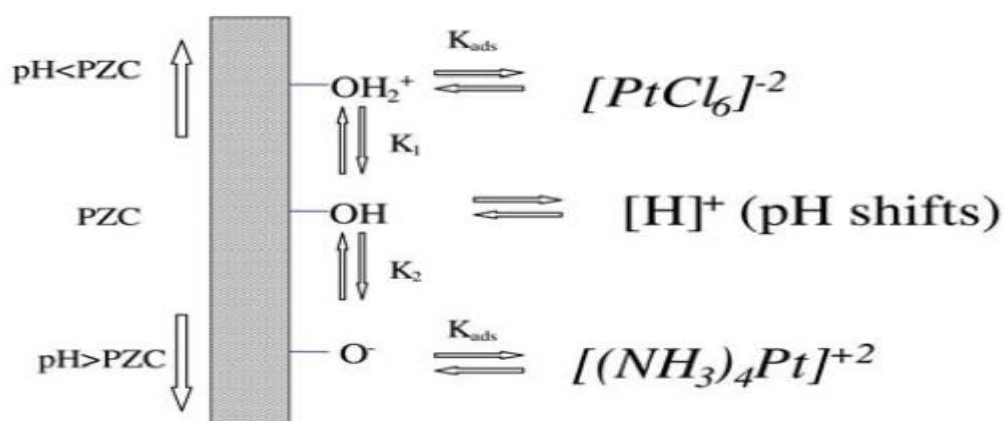


Figure 2.14: Illustration of Ion Adsorption on Solid Support with Adjusted pH (Zhu *et. al.*, 2009)

However, the strong buffering capacity of oxide support surface at incipient wetness would tend to adjust the pH back to PZC by pH shifts. This calls for the need to acidify or basify the support surface to a greater extent away from its PZC. Hence the PZC and final pH after the adsorption on support has to be determined to know the right initial pH to carry out the CEDI. In order to achieve this, Cao *et. al.* (2014) reported that solutions of varying pH in the range of pH 2 to pH 13 were prepared and carbon black support was added according to surface loading desired. Zhu *et.al.* (2013) described that surface loading could be computed by the following formula:

$$SL \left(\frac{\text{m}^2}{\text{L}} \right) = \frac{\text{BET surface area} \left(\frac{\text{m}^2}{\text{g}} \right)}{\text{pore volume} \left(\frac{\text{L}}{\text{g}} \right)}$$

The final pHs of the solutions after shaking for 1 hour were recorded. A graph of final pH against initial pH was plotted and the plateau formed on the curve would indicate the PZC of the support.

As for the decision on the initial pH to carry out CEDI, Cao *et. al.* conducted a preliminary adsorption survey by impregnating the supports at varying pH between pH 2 to pH 13 and the concentration of metal phase before and after were tested by ICP-OES. Adsorption density was calculated using results from ICP-OES by the formula reported by Hao *et. al.* (2003) as following:

$$\Gamma = \frac{C_{\text{adsorbed}} V_L}{m_{\text{ox}} S_{\text{ox}}}$$

The final pH that showed the highest adsorption density would be the optimum final pH for CEDI. During the actual CEDI, the metal precursor solution was adjusted to the initial pH chosen and added dropwise to the supports. The catalysts were then dried in room temperature and reduced in flow of hydrogen gas.

2.4.3 Heat Treatment

Typically, solid catalysts formed are subjected to heat treatments consisting of drying, calcination and reduction. Heat treatment is crucial to ensure that the catalyst active phase is ready for catalysis while concurrently plays a role in varying the performance of the catalyst. The first heat treatment step is drying in order to remove solvents for the metal precursors from the catalyst. It is done by heating the catalysts with static or flowing dry air to the boiling point of the solvent or lower temperatures for gentle drying. (Marceau, 2009) The removal of solvents would increase the concentration of metal precursors up to saturation and crystallisation point in the catalyst. However, elimination of solvent which has low viscosity would tend to carry the metal solute along and result in segregation of metal precursors to the pore mouths, forming the egg-shell distribution. Nevertheless, Li *et. al.* (1994) reported that when using nickel(II) nitrate hexahydrate as the precursor, Ni/ γ -Al₂O₃ with egg-shell distribution is only achieved by fast heating up to 200°C.

After drying, the catalyst would typically be calcined by prolonged heating at high temperatures. The temperature of calcination in air is generally above its catalytic reaction temperature or regeneration temperature. An array of processes occur in the catalyst during calcination including the loss of chemically bonded water molecules or CO₂, texture modification by sintering whereby small particles combine to form larger ones, structure modification, active phase generation and also stabilisation of mechanical properties. (Perego, 1997) The effect of calcination is well demonstrated in heating of aluminium hydroxide. When aluminium hydroxide is calcined at above 300°C, a series of phase changes take place along with loss of hydroxyl groups and water, resulting in formation of oxides with γ -, δ - or η - phase which are good binder and support for catalyst preparation.

After calcination, the metal precursors which are in metal hydroxalcite form are turned into metal oxides. The metal oxides then have to be reduced by flows of hydrogen gas at elevated temperature to form the active metal phase ready for catalytic reaction. Bartholomew and Farrauto (1976) reported that impregnated catalyst generally has higher degree of reduction compared to catalyst prepared by precipitation. They also found that the reducibility and dispersion of nickel in Ni/ γ -

Al_2O_3 catalyst was significantly higher for those without calcination in comparison with those that were calcined beforehand. This was because the NiO reacts with Al_2O_3 during high temperature calcination to form very stable NiAl_2O_4 spinel which could not be reduced even under very high temperature reduction condition. During reduction, hydrogen reacts with nickel oxide to produce water which is driven off with a slow heating rate and carried away by the flow of hydrogen to minimise sintering effect. It was also mentioned that catalyst dispersion could be controlled by manipulating the amount of water removed by drying or by controlling the heating rate and partial pressure during reduction.

Table 2.3: Summary of calcination and reduction conditions for synthesis of Ni/ γ - Al_2O_3 from literatures.

Author	Method	Calcination Condition	Reduction Condition
Broecker <i>et al.</i> (1975)	Co-precipitation	350°C for 20 hours	400°C to 470°C for 20 hours
Subramani V. (2006)	Co-precipitation	450°C for 5 hours	N/A
Li <i>et al.</i> (2005)	Co-precipitation	600°C for 3 hours	550°C for 1 hour
Adkins H. (1930)	Co-precipitation	450°C for 1 hour	N/A

Bartholomew C.H. and Farrauto R.J. (1976)	Dry Impregnation	400°C for 1 or 2 hours	Heat at 5°C/min to 230°C and hold for 1 hour, then heat to 480°C and hold for 10 hours
Chen <i>et. al.</i> (1988)	Dry Impregnation	600°C for 2.5 hours	400°C to 700°C for 0.5 hours to 9 hours
Simpson H.D. (1995)	Dry Impregnation	480°C to 550°C for 0.5 hours	N/A
Vogelaar B. <i>et. al.</i> (2010)	Dry Impregnation	N/A	Heat at 10°C/min to 450°C for 4 hours

2.5 Characterisation of Catalysts

Characterisation of catalysts is vital in determining the desirable traits of a catalyst that are contributing to good catalytic performance. These characteristics could in turn provide guideline on viability of the synthesis methods employed. Generally, catalysts are characterised in terms of its surface properties and fine structure. Surface properties are commonly determined by adsorption method while electron spectroscopy is used to analyse the fine structure.

Surface properties that are of interest include metal dispersion, active phase surface area and metal particle size. As these characteristics involve the active phase of the catalyst, chemisorption method has to be applied instead of physisorption. One of the chemisorption analyses available is pulse chemisorption analysis using TPDRO whereby adsorbates such as hydrogen or oxygen gas are pulsed into the carrier gas passing through the catalyst sample. The first few pulses would be completely adsorbed and the successive pulses are added until no adsorption occurs anymore (Haber *et. al.*, 1995). The amount of gas adsorbed is the differential area between the first few smaller peaks and the successive larger peaks (Nakai and Nakamura, 2003). The surface properties could be computed from the amount of gas adsorbed through the formulas presented in Table 2.4 below.

Table 2.4: Formulas for Surface Properties Calculation.

Surface Properties	Formula	Remarks
Metal Dispersion, D (%) (Lowell <i>et. al.</i> , 2004)	$D = \frac{\text{Moles of metals on sample surface}}{\text{Moles of total metals present in sample}}$ $= n \times \frac{V_{\text{adsorbed}}}{V_{\text{gas,s.t.p.}}} \text{ moles/g}$ $= \frac{M}{mw \times 100} \text{ moles/g}$	n = stoichiometry factor M = metal loading (wt%) mw = molecular weight

<p>Metal Surface Area, A_m (m^2/g)</p> <p>(Lowell <i>et. al.</i>, 2004)</p>	<p>$A_m = \text{total surface metal atoms} \times \text{cross sectional area of metal atom}$</p> $= n \times \frac{V_{\text{adsorbed}}}{V_{\text{gas,s.t.p.}}} \times N_A \times a$	<p>$N_A = \text{Avogadro's number}$</p> <p>$a = \text{cross sectional area of metal atom}$</p>
<p>Metal Average Particle Size, d_p (nm/atom)</p> <p>(Bergeret <i>et. al.</i>, 2008)</p>	$d_p = 6 \times \frac{V_m/a_m}{D}$ $a_m = \frac{1}{n_s}$ $V_m = \frac{\text{atomic weight}}{\rho N_A}$	<p>$D = \text{dispersion}$</p> <p>$a_m = \text{area of an atom on sample surface}$</p> <p>$n_s = \text{mean number of atoms on sample surface}$</p> <p>$V_m = \text{volume occupied by an atom}$</p> <p>$\rho = \text{atomic mass density}$</p> <p>$N_A = \text{Avogadro's number}$</p>

On the other hand, the fine structure of catalyst could be characterised by XRD and SEM-EDX analyses. These analytical methods operate based on the concept of electron spectroscopy. They provide identification of phases and structural information on crystals, direct images of sample surfaces and surface elemental composition. (Haber *et. al.*, 1995)

CHAPTER 3

METHODOLOGY

3.1 Materials

For synthesis of catalyst, nickel nitrate hexahydrate, $\text{Ni}(\text{NO}_3)_2 \cdot 6\text{H}_2\text{O}$ was used as the precursor for nickel active phase while iron (III) nitrate nonahydrate, $\text{Fe}(\text{NO}_3)_3 \cdot 9\text{H}_2\text{O}$ was used as precursor for iron active phase.

In co-precipitation method, aluminium nitrate nonahydrate, $\text{Al}(\text{NO}_3)_3 \cdot 9\text{H}_2\text{O}$ was used as the alumina precursor and sodium bicarbonate, NaHCO_3 as the precipitating agent. For synthesis of impregnated catalyst by CEDI and dry impregnation, commercial γ -alumina pellets with surface area of $300 \text{ m}^2/\text{g}$ were used as the catalyst supports. All the chemicals used were under the brand of Bendosen purchased from Progressive Scientific Sdn. Bhd.

Three types of commercial nickel catalysts were obtained from Southern Acids Industries. They come in pellet form coated with saturated fats to prevent oxidation.

3.2 Determination of Point Zero Charge (PZC) for γ -Al₂O₃ Pellets

In order to synthesise catalyst with charge enhanced dry impregnation method (CEDI), the PZC of the γ -alumina used has to be determined as the preliminary step in deciding the initial pH to be used during the CEDI. The determination test for PZC was conducted through the following steps:

- a) The γ -alumina pellets were crushed using pestle and mortar.
- b) Deionised water solutions with varying pH of 100 ml each were prepared by using HNO₃ and NaOH. Ten solutions with different pH were prepared. The pH of the water solutions were measured and recorded as initial pH.
- c) γ -alumina with surface loading of 150 m²/L was prepared by weighing 0.05 g of crushed γ -alumina and adding into a beaker containing 100 mL of one of the pH adjusted water solution. (Calculations of surface loading are presented in Appendix A).
- d) Step (c) was repeated for each of the beakers containing 100 mL of water solution with the other 9 initial pH values.
- e) The mixtures were stirred for 8 minutes at room temperature.
- f) The mixtures were then allowed to stabilise without stirring for 10 minutes.
- g) The final pH of the solution with crushed alumina was recorded.
- h) Steps (c) to (g) were repeated for γ -alumina surface loadings of 300 m²/L and 600 m²/L. The surface loadings were prepared by changing the volume of water solution to 50 mL and 25 mL respectively while holding the mass of γ -alumina constant at 0.05 g. The surface loadings were varied in order to get a more accurate PZC reading and take into account any effect of surface loading on its PZC.
- i) A graph of final pH versus initial pH was plotted for all the surface loadings.

3.3 Determination of pH for Optimal Adsorption

The final pH after adsorption of active phase onto the γ -alumina support has to remain below its PZC to prevent desorption. Hence, the determination of initial pH for optimal adsorption has to take into account the buffering capacity of the oxide support so that the resulted final pH would still be below the PZC. The final pH taking into account of oxide buffering effect was surveyed by the following steps:

- a) The γ -alumina was crushed using pestle and mortar.
- b) 20 ppm of $\text{Ni}(\text{NO}_3)_2 \cdot 6\text{H}_2\text{O}$ solution was prepared over the pH range of 1 to 14 using HNO_3 and NaOH . 30 mL of $\text{Ni}(\text{NO}_3)_2 \cdot 6\text{H}_2\text{O}$ solution was prepared for each pH level.
- c) 20 ppm of $\text{Fe}(\text{NO}_3)_3 \cdot 9\text{H}_2\text{O}$ solution was prepared over the pH range of 1 to 14 using HNO_3 and NaOH . 30 mL of $\text{Fe}(\text{NO}_3)_3 \cdot 9\text{H}_2\text{O}$ solution was prepared for each pH level.
- d) 0.03 g of crushed γ -alumina was weighed and added into 15 mL of each of the pH adjusted $\text{Ni}(\text{NO}_3)_2 \cdot 6\text{H}_2\text{O}$ and $\text{Fe}(\text{NO}_3)_3 \cdot 9\text{H}_2\text{O}$ solutions prepared in step (b) and (c) in order to prepare γ -alumina surface loading of $600 \text{ m}^2/\text{L}$.
- e) Each of the mixtures was mixed thoroughly for 1 hour.
- f) Final pH values for each of the mixtures were measured.
- g) The slurry solutions were filtered to remove the suspended γ -alumina.
- h) The filtered solution was then measured for final concentration using inductively coupled plasma optical emission spectroscopy (ICP-OES, Perkin-Elmer Optima 7000 DV).
- i) Initial pH adjusted solutions of $\text{Ni}(\text{NO}_3)_2 \cdot 6\text{H}_2\text{O}$ and $\text{Fe}(\text{NO}_3)_3 \cdot 9\text{H}_2\text{O}$ from step (b) and (c) which had not been contacted with γ -alumina, at each pH, were measured for initial concentration using the ICP-OES.
- j) A graph of adsorption density versus final pH was plotted.

3.4 Synthesis of Catalyst

The Ni-Fe/ γ -Al₂O₃ catalyst was prepared separately by the following methods: charge-enhanced dry impregnation method, dry impregnation method and co-precipitation method.

3.4.1 Charge-Enhanced Dry Impregnation Method (CEDI)

The total metal loading was set at 2 wt% comprising of equimolar nickel and iron precursors content. The detailed calculation is provided in Appendix B. The following outline the steps involved for catalysts prepared using CEDI method:

- a) 0.7616 g of Ni(NO₃)₂ · 6H₂O and 1.0582 g of Fe(NO₃)₃ · 9H₂O were dissolved in 14.7 ml of deionised water. The volume of liquid was equivalent to the pore volume of the pellets to ensure incipient wetness for dry impregnation to take effect.
- b) Just enough amount of NaOH was added to adjust the impregnating solution pH to pH 14.
- c) The impregnating solution was added dropwise to 14.7 g of alumina pellets and kept in a closed vessel for 2 hours.
- d) The impregnated pellets were dried in oven with static air at 100°C for 8 hours.
- e) The pellets were calcined at 350°C for 8 hours.

3.4.2 Dry Impregnation Method

The total metal loading was set at 20 wt% comprising of equimolar nickel and iron precursors content. The detailed calculation is provided in Appendix C. The following outline the steps involved for catalysts prepared using DI method:

- a) 7.6165 g of $\text{Ni}(\text{NO}_3)_2 \cdot 6\text{H}_2\text{O}$ and 10.5817 g of $\text{Fe}(\text{NO}_3)_3 \cdot 9\text{H}_2\text{O}$ were dissolved in 13.2 ml of deionised water. The volume of liquid was equivalent to the pore volume of the pellets plus 10% to ensure incipient wetness for dry impregnation to take effect.
- b) The impregnating solution was added dropwise to 12 g of alumina pellets and kept in a closed vessel for 2 hours.
- c) The impregnated pellets were dried in oven with static air at 100°C for 8 hours.
- d) The pellets were calcined at 450°C for 8 hours.

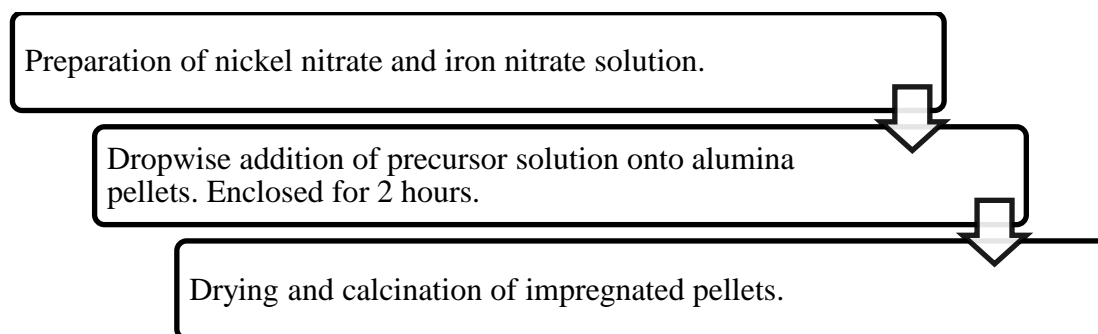


Figure 3.1: Summary of Dry Impregnation Method.

3.4.3 Co-Precipitation Method

Based on the chemical equation extracted from patent by Broecker *et. al.* (1973), the molar ratio of metal precursor was equally divided to achieve equimolar bimetallic precursors. Using aluminium nitrate nonahydrate as basis (1 mol), 1.5 moles of each metal precursor (nickel nitrate and iron nitrate) and 10 moles of sodium bicarbonate were mixed to form the catalyst precursor. A factor of 15 was used to scale down the

amount of catalyst as proposed by Broecker *et. al.* (1973). The detailed calculation is provided in Appendix D.

- a) The materials involved were measured using electronic microbalance with weight specifications as follow:

Materials	Molar Ratio	Weight (g)
Nickel Nitrate Hexahydrate	1.5	29.08
Iron(III) Nitrate Nonahydrate	1.5	40.40
Aluminium Nitrate Nonahydrate	1	25.01
Sodium Bicarbonate	10	56.01

- b) The measured nickel nitrate, iron(III) nitrate and aluminium nitrate were added to 133.33 ml of deionised water to form Solution 1 with concentration of 2 mol/L.
- c) The measured sodium bicarbonate was added to 333.33 ml of deionised water to form Solution 2 with concentration of 2 mol/L.
- d) 41.67 ml of deionised water was added into a conical flask which acts as the precipitating vessel.
- e) All the solutions prepared were heated to 80°C.
- f) Solution 1 was added to the precipitating vessel until pH 5.
- g) Solution 1 and 2 were added slowly to the precipitating vessel while maintaining the pH between pH 4.5 and 5.5.
- h) The remaining Solution 2 was added only after Solution 1 had all been added to reach pH 6 at the end.
- i) The precipitating solution was stirred at 80°C for a further 15 minutes.
- j) The precipitated slurry was filtered with the aid of filter paper and a vacuum ejector.
- k) The precipitated slurry was washed with 4 L of deionised water.
- l) The precipitate was dried in the oven at 120°C for 3 hours.
- m) The dried precipitate was calcined in the furnace at 350°C for 20 hours.

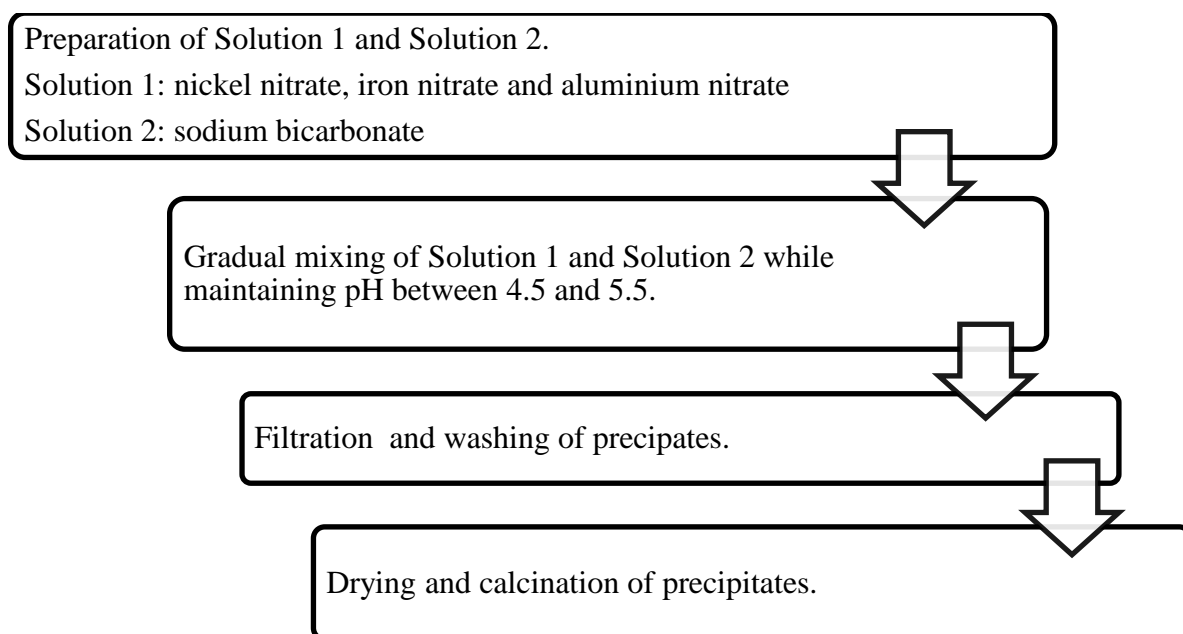


Figure 3.2: Summary of Co-Precipitation Method.

3.5 Characterisation

The synthesised and commercial catalysts were subjected to various analyses in order to determine their physical characteristics which could be used to predict their catalytic performance and help in understanding the catalytic process. Table 3.1 below summarises the type of analyses conducted on each of the samples.

Table 3.1: Summary of Characterisation Analyses on Each Sample.

Type of Catalyst	Type of Analysis				
	XRD	TPR	Pulse Chemisorption	SEM	EDX
Dry Impregnation Ni-Fe	√	√	√	√	√
Co-Precipitation Ni-Fe	√	√	√	√	√

Dry Impregnation Ni-Zn	√	√	√	√	√
Co- Precipitation Ni-Zn	√	√	√	√	√
A	-	√	√	√	√
B	-	√	√	√	√
C	-	√	√	√	√

3.5.1 X-ray Diffraction (XRD) Analysis

X-ray Diffraction (XRD) was used to determine the crystallite size, lattice spacing and the phases present in the catalyst. The catalyst sample was crushed to powder form and packed evenly in the sample holder until a smooth surface was obtained. The analysis employed a Shimadzu LabX XRD-6000 with Cu K α radiation ($\lambda = 1.54 \text{ \AA}$) operated at 30 mA and 40 kV. The scan was carried out from 3° to 80° at scanning rate of 2°/second in room temperature of 25°C.



Figure 3.3: Shimadzu LabX XRD-6000 Machine

3.5.2 Temperature Programmed Reduction (TPR) Analysis

Temperature programmed reduction (TPR) was conducted to determine the optimum reduction temperature for the catalyst. It was done by determining the amount of hydrogen gas used to react with the oxygen liberated from catalyst sample when heated at different temperatures. Thermo Scientific TPDRO 1100 with built-in thermal conductivity detector (TCD) was employed in this analysis. The sampling size for each run is 0.02 g of crushed catalyst sample. Pre-treatment was carried out before the reduction process whereby the samples were cleaned with nitrogen gas flow of 20 cm³/min starting from room temperature to 200°C with heating ramp of 10°C/min and held for 10 minutes. For the TPR analysis, the sample was purged with 5.47% hydrogen in nitrogen gas at 25 cm³/min starting from room temperature to 1000°C with heating ramp of 5°C/min.

3.5.3 Pulse Chemisorption Analysis

Pulse chemisorption analysis was done to determine the dispersion of metal active sites on catalyst surface, surface area of metal active sites as well as the average metal particle size. This was enabled by detecting the amount of hydrogen gas chemically adsorbed on the metal active sites. Thermo Scientific TPDRO 1100 with built-in thermal conductivity detector (TCD) was employed in this analysis. The sample size used was 0.015 g. The sample undergoes three stages of conditioning in-situ prior to pulse chemisorption as summarised in Table 3.1 below. The pulse chemisorption analysis was conducted with 20cm³/min hydrogen gas at 40°C. Ten pulses were done with time between pulses being 15 minutes.

Table 3.2: Conditioning Stages Prior to Pulse Chemisorption.

Stage	Gas Used	Gas Flow Rate (cm ³ /min)	Ramp (°C/min)	Starting T (°C)	Target T (°C)	Holding Time (min)
Sample degassing	Nitrogen	20	10	-	120	60
Reduction	5.47% Hydrogen in nitrogen gas	20	20	-	400	60
Degassing after reduction	Nitrogen	20	1	390	400	120



Figure 3.4: Thermo Scientific TPDRO 1100

3.5.4 Scanning Electron Microscopy with Energy Dispersive X-ray Spectroscopy (SEM-EDX)

Scanning Electron Microscopy (SEM) was used to characterise the surface morphology and topography of the catalyst sample. A Hitachi S-3400N was employed at 20 kV with varying magnification. The crushed catalyst samples were coated with palladium and gold with Emitech Sputter Coater beforehand to increase its conductivity. Energy Dispersive X-ray Spectroscopy (EDX) was also carried out using the same machine in order to investigate the elemental composition of the sample. Results from three different spots on the catalyst were obtained and the average reading was calculated.



Figure 3.5: Hitachi S-3400N SEM-EDX Machine.

CHAPTER 4

RESULTS AND DISCUSSIONS

4.1 Determination of Point Zero Charge (PZC) for γ -Al₂O₃ Pellets

Figure 4.1 below shows the results obtained from the determination of point zero charge for the γ -Al₂O₃ pellets. A plateau could be observed for every surface loading which typically occurred in the range of pH 7 to pH 9. The occurrence of plateau shows that the different initial pH tends to shift back to one final pH point. This is attributed to the buffering effect of the oxide support that would shift the pH back to its PZC. The plateau for each surface loading was averaged out to arrive an average PZC of 7.2. This is fairly in accordance to PZC of alumina reported by Zhu *et. al.* (2013), Park and Regalbuto (1995) and Spieker and Regalbuto (2000) which are in the range of pH 7.7 to pH 8.5. The raw data obtained is provided in Appendix E.

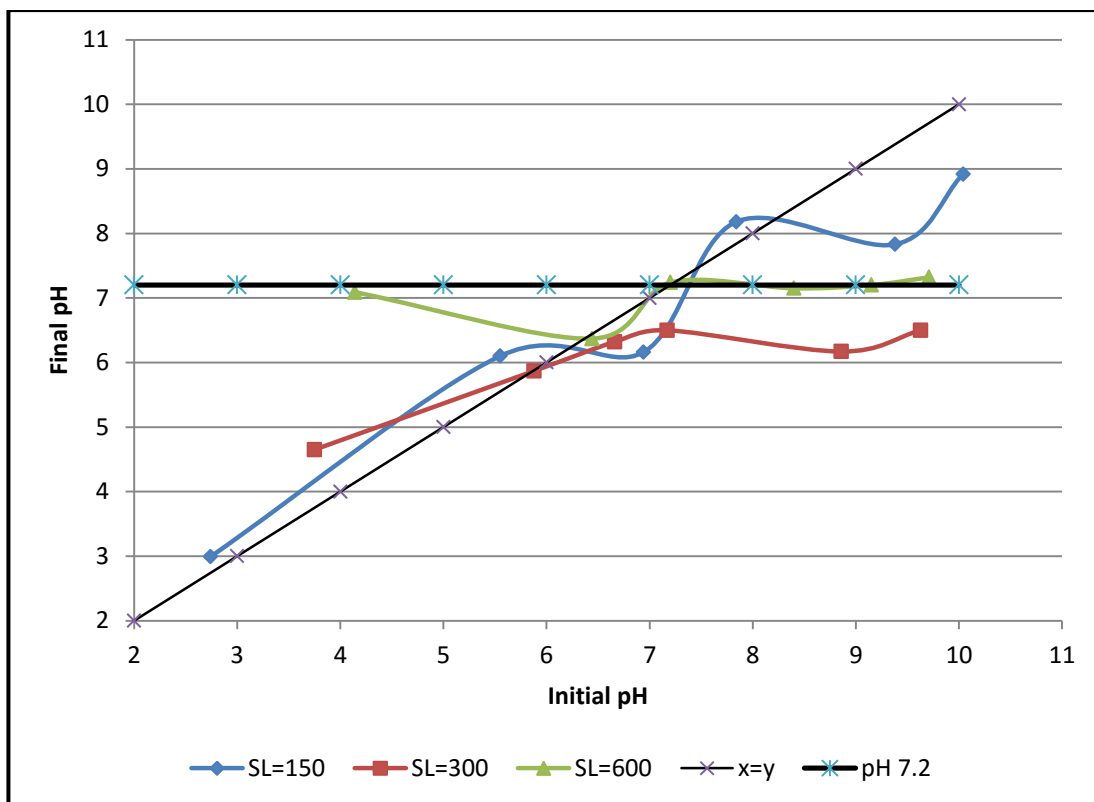


Figure 4.1: Equilibrium pH of γ -alumina at Different Surface Loading.

Shifts in pH occur all along the curves in Figure 4.1 but vary in magnitude. Generally, those with initial pH lower than the PZC would shift upwards while those with initial pH higher than PZC would shift downwards, both of which will converge to the PZC. This is because the hydroxyl groups on the alumina surface would be protonated by H^+ ions from bulk solution in the initial low pH environment hence decreasing the amount of free H^+ ions in the bulk solution and raising the pH of bulk solution. The opposite effect would occur on those with initial pH higher than PZC whereby OH^- ions from the basic bulk solution would deprotonate the hydroxyl groups on alumina surface which subsequently decrease the pH of bulk solution towards PZC.

In Figure 4.1, the $x = y$ line represents situation with no pH shift whereby initial pH equals to final pH. The spacing between the curves and the $x = y$ line enables the comparison of tendency for pH shift at different surface loading. The further the curves away from the $x = y$ line, the more prominent the pH shift. By comparison, the curve of $SL=600 \text{ m}^2/\text{L}$ is furthest away from $x = y$ line and nearest

to the PZC=7.2 line among the three curves. It could be inferred that alumina with higher surface loading experienced larger pH shifts than those with lower surface loading. This could be due to the abundance of hydroxyl groups on oxide surface at higher surface loading which far outnumbers the H^+ and OH^- ions in the bulk solution, resulting significant buffering effect and high tendency for the pH to stay at its PZC.

As depicted in Figure 4.1, the pH shift at the lower extreme end of the lower surface loading curves is the least prominent due to its very close proximity to the $x = y$ line. This is attributed to the abundance of H^+ ions in very acidic bulk solution whereby even after protonation of the oxide surface that removed a number of H^+ ions from the bulk solution, the amount of H^+ ions remaining in bulk solution is still very significant and sufficient to maintain the low pH environment. At this point, the oxide support surface is considered to be sufficiently charged as all of the hydroxyl groups have been protonated and the oxide support is in favour of electrostatic adsorption with metal ions of opposite charge. This phenomenon should have occurred similarly in the higher extreme end of the curve as well in accordance to observation at pH 14 by Zhu *et. al.* (2013). However it is not clearly seen in Figure 4.1 as the highest initial pH available was not up to pH 14.

In summary, the PZC of the γ -alumina pellets used was found to be at pH 7.2 and the alumina must be sufficiently charged with an extreme pH that would overcome the buffering effect to facilitate electrostatic adsorption. Nevertheless, the optimum pH for strong electrostatic adsorption of metal ions might not be the extreme pH. Therefore, the actual optimum pH is investigated in the following section by an adsorption survey.

4.2 Determination of pH for Optimal Adsorption

The empirical result for determination of pH for optimal adsorption is shown in Figure 4.2 below. The optimum pH for adsorption is the pH that produces the highest

adsorption density. In Figure 4.2, the highest peak for nickel is at pH 7.74 while for iron it is at pH 10.58.

In order to obtain the optimum pH for the adsorption of both metals, the point where the highest peak for nickel and second highest peak for iron are in close proximity is chosen. This is represented by the dotted vertical straight line at final pH of 7.7. In addition, this point is chosen because near the highest peak of iron, the nickel curve has very low peak and results in a less satisfactory combination compared to the abovementioned point. The raw data obtained from the experiment is provided in Appendix F together with the calculation of adsorption density.

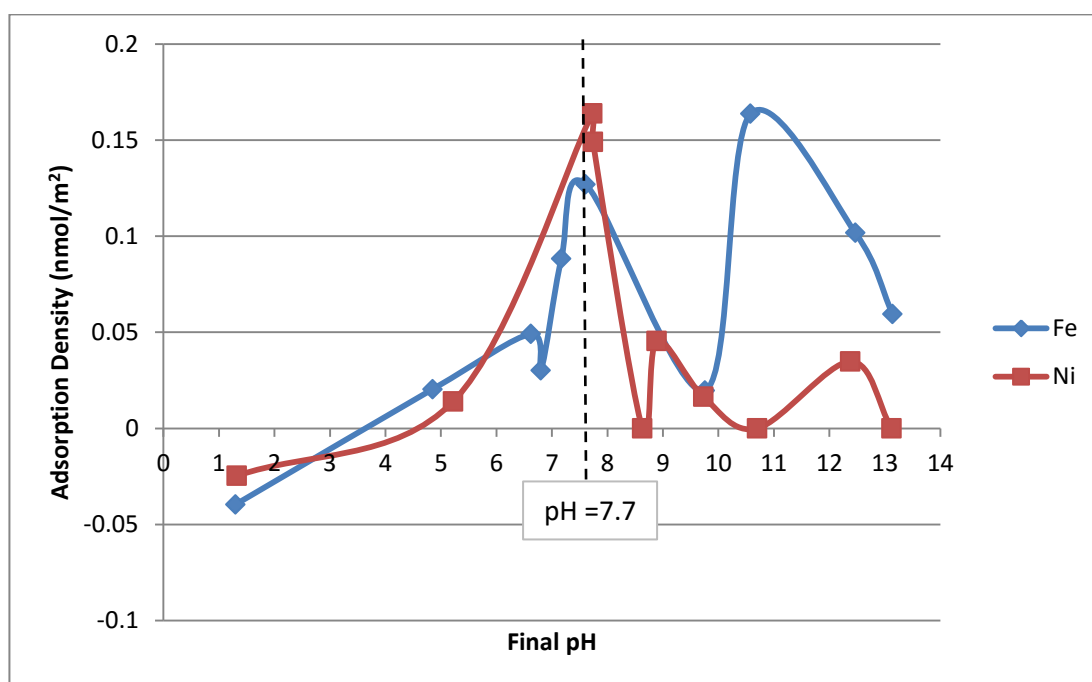


Figure 4.2: Graph of Adsorption Density against Final pH for Nickel and Iron on γ -Alumina with $SL= 600m^2/L$.

In order to achieve the optimum final pH of 7.7, the initial pH has to be above pH 7 according to the pH shift for $SL= 600m^2/L$ in Figure 4.1. However, from a theoretical standpoint, if $pH = 7.7$ is used for the initial impregnating solution, this will be too close to the PZC ($pH = 7.2$) and therefore the alumina support is not charged and the impregnation would just be conventional dry impregnation instead

of being charge enhanced. Knowing this, theoretical calculation was employed to help decide the initial pH to be used for dry impregnation.

Summary of the theoretical calculation is presented in Table 4.1 below while the detailed calculation steps are shown in Appendix G. The specific surface area and pore volume of alumina support were provided by supplier while hydroxyl density constant is obtained from literature by Zhu *et. al.* (2013). Mass of alumina to be used for synthesis was set as 14.7 g. Based on the theoretical calculation, the minimum amount of hydroxide ions required to fully deprotonate the hydroxyls on alumina support surface would result in bulk solution with initial pH 14.6. The alumina support surface has to be deprotonated to enable electrostatic adsorption between opposite charges as the nickel and iron are both positively charged ions.

Table 4.1: Theoretical Calculation for Initial pH of Bulk Impregnating Solution.

Specific surface area of support	300 m ² g ⁻¹
Pore volume of support	1 cm ³ g ⁻¹
Hydroxyl density	8 OH nm ⁻²
pOH	-0.6
pH (pH + pOH = 14)	14.6
<u>Number of hydroxyls on support surface</u>	
Mass of alumina	14.7 g
Conversion from nm ² to m ²	1.00 × 10 ¹⁸ nm ² m ⁻²
Avogadro's Number	6.02 × 10 ²³ mol ⁻¹
Number of hydroxyls	0.0586 moles
<u>Number of hydroxide ions from bulk solution</u>	
Volume of solution	1.47 × 10 ⁻² L
OH ⁻ concentration	3.98474 mol/L
Number of hydroxide ions	0.0586 moles

By putting together the empirical and theoretical findings, it was decided that the suitable initial pH to be used for CEDI synthesis method is pH 14. This would allow a margin of safety while ensuring that the alumina support surface is fully deprotonated and carries negative charge to adsorb the positively charged nickel and iron ions. In summary, the final pH for optimal adsorption is pH 7.7 as determined

empirically. However, pH 14 is chosen as the initial pH based on theoretical calculation as this allows the alumina support to be sufficiently charged to allow electrostatic adsorption of nickel and iron to the support.

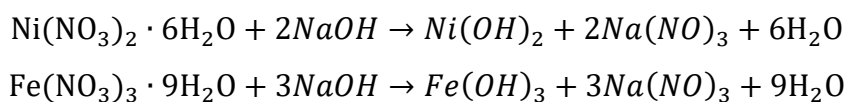
4.3 Observation from Synthesis of Catalyst

The catalyst was prepared by charge enhanced dry impregnation method, dry impregnation method and co-precipitation method. The unique findings during synthesis of catalyst by CEDI were specifically presented in the following section.

4.3.1 Charge Enhanced Dry Impregnation Method

The synthesis started off with preparation of the impregnating solution by dissolving the calculated amount of nickel nitrate hexahydrate and iron nitrate nonahydrate into 13.5 ml of deionized water. During adjustment of pH for the impregnating solution, it was observed that upon addition of NaOH solution into the impregnating solution, dark greenish-brown precipitation was formed. Attempts made to dissolve the solids by heating up the solution to boil were not showing positive effects. In view of that, the catalyst preparation with this method was halted.

The possible reactions involved during the abovementioned pH adjustment are as shown in the following chemical equation.



The precipitations formed are nickel hydroxide and iron hydroxide which are both insoluble in water. The precipitation effect was so prominent due to the addition of very concentrated NaOH for pH adjustment up to pH 14. This was not encountered during the optimum pH for adsorption survey as the amount of NaOH added was not as significant. The NaOH added during this preparation was in high concentration as

only a tiny amount of deionized water is allowed for the CEDI method. Since the free ionic form of nickel and iron could not be formed in the aqueous impregnating solution for electrostatic adsorption with hydroxyl groups on alumina surface, the impregnation could not be conducted.

Although charge enhanced dry impregnation method has been proven to be effective in synthesizing Pt-Pd/ γ -Al₂O₃ catalyst by Zhu *et. al.* (2013) and also carbon-supported Pd/Mo catalyst by Cao *et. al.* (2014), it did not work well with the current synthesis of Ni-Fe/ γ -Al₂O₃ catalyst. This could be due to the difference in the surface charging condition. For Pt-Pd/ γ -Al₂O₃ catalyst by Zhu *et. al.* (2013), the metal ions formed were $PtCl_6^{2-}$ and $PdCl_6^{2-}$ which are both anions that require the alumina surface to be protonated by addition of acids. Meanwhile, in current synthesis, the metal precursor ions are Ni²⁺ and Fe³⁺ which are cations and the alumina surface needs to be deprotonated by addition of base. Therefore, the issue of insoluble nickel hydroxide and iron hydroxide precipitates is specific to the current synthesis due to the need to add a strong base, NaOH for pH adjustment.

In summary, insoluble nickel hydroxide and iron hydroxide were formed when NaOH was added to the impregnating solution. However, the presence of hydroxide ions was inevitable due to the need to sufficiently basify the impregnating solution for deprotonation of alumina surface. It was deduced that charge enhanced dry impregnation of cation metal precursor was unable to proceed until a way to prevent the formation of insoluble metal hydroxides is found.

4.3.2 Dry Impregnation Method

The alumina pellets were impregnated at incipient wetness to form Ni-Fe catalysts. The white pellets turned into dark brown colour following the dropwise addition of impregnating solution. After oven drying, the pellets showed lighter shade of brown and no longer tend to attach to the wall of container. Subsequent calcination at 450°C for 8 hours turned the catalyst pellets into dark brown colour. The catalysts showed

static charge interaction with the wall of the plastic petri dish in which they were contained. They were seen attaching to the walls or “popping” in random directions when the lid of petri dish was closed. The catalyst prepared by dry impregnation is shown in Figure 4.3 below.



Figure 4.3: Catalyst synthesised by dry impregnation method before drying (left) and after calcination (right).

4.3.3 Co-Precipitation Method

Co-precipitation method was successfully employed to prepare Ni-Fe/ γ -alumina catalyst. The precipitates formed were seen to have very fine particles and light brown in colour. After calcination at 350°C for 20 hours, the catalysts became dark brown colour in the form of fine powder. The aluminium carbonates were turned into γ -alumina phase due to calcination above 300°C as reported by Perego (1997) or above 350°C by Trueba (2005). Approximately 10 g of catalysts were synthesised using this method.



Figure 4.4: Catalyst synthesised by co-precipitation method after drying (left) and after calcination (right).

4.4 Characterisation

The catalyst synthesised were subjected to characterisation tests in order to investigate the effect of different synthesising method on the catalyst. The characterisation results obtained from XRD analysis, TPR analysis, Pulse Chemisorption analysis and SEM-EDX analysis are presented in the following sections.

4.4.1 X-ray Diffraction (XRD) Analysis

The XRD analysis results for Ni-Fe/ γ -alumina catalyst prepared by dry impregnation are shown in Figure 4.5 while the results for those from co-precipitation method are presented in Figure 4.6 below. XRD diffractograms for both of the synthesised catalysts are quite similar with three peaks detected. The peaks in both of methods are in close proximity of each other. Peaks of dry impregnation method are detected at 37.3° , 45.9° and 66.8° while those in co-precipitation method are seen at 37.8° ,

45.3 ° and 66.6 °. These peaks show the presence of γ -alumina phase in accordance with γ -alumina phase XRD peaks at 37.2 °, 45.6 ° and 66.9 ° -reported by Rozita *et al.* (2010). In addition, this is further confirmed by the search and match system which shown detection of aluminium oxide for both of the samples. The raw data for XRD and search and match results are presented in Appendix J.

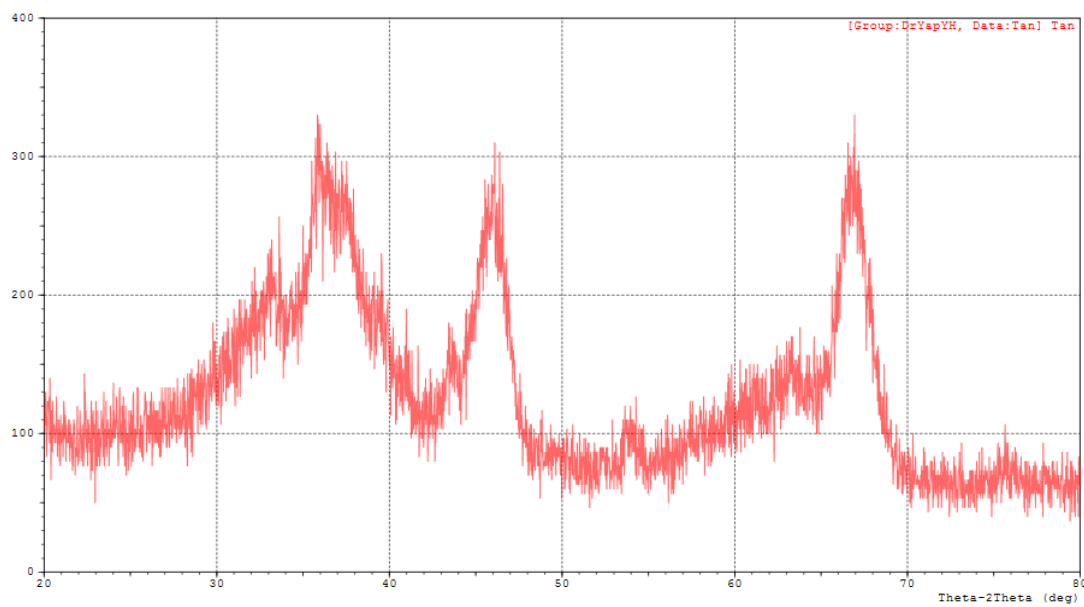


Figure 4.5: XRD Diffractogram for Ni-Fe/ γ -alumina by Dry Impregnation.

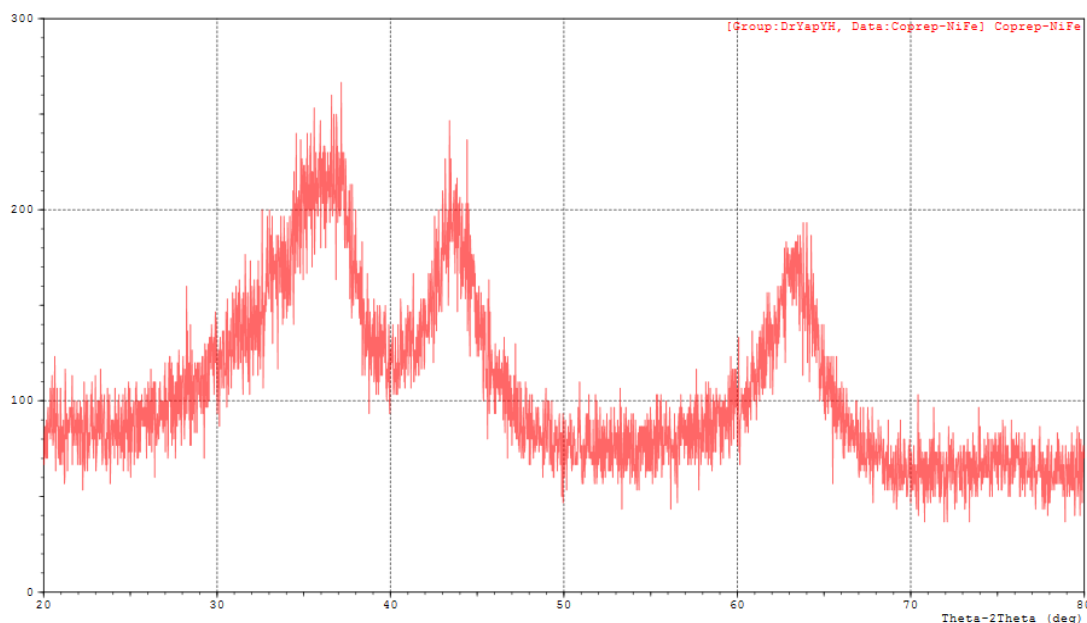


Figure 4.6: XRD Diffractogram for Ni-Fe/ γ -alumina by Co-Precipitation.

From the XRD diffractograms, the samples are also found to be low in crystallinity based on the low and broad peaks in their diffractograms. This shows that the synthesised catalysts are generally more amorphous (especially the metal phases) as no peaks corresponding to the metals are observed. The search and match system also did not return any matches related to the metal phases except for some minor calcium iron oxide in the co-precipitation method sample. Nevertheless, when compared between the Ni-Fe catalysts, the XRD peaks of Ni-Fe catalyst by dry impregnation method are more sharp and distinct, indicating a relatively higher crystallinity as seen in Figure 4.7.

On the other hand, the XRD results of synthesised Ni-Fe/ γ -alumina catalysts are compared with those of Ni-Zn/ γ -alumina catalyst prepared using the same methods by another student – Tan Wen Hsiung. The overlay graphs for both dry impregnation and co-precipitation method is shown in Figure 4.7. For both of the methods, Ni-Zn catalysts showed sharper and higher peaks denoted in blue compared to Ni-Fe catalysts. This indicates that the combination of nickel and zinc in the catalyst could achieve higher crystallinity than nickel and iron regardless of the synthesis method. Higher crystallinity is also an indication of higher structure stability according to Tong *et. al.* (2007) whom reported that the more crystalline catalyst could maintain its catalytic performance over more reaction cycles than the less crystalline ones.

Furthermore, the Ni-Zn catalysts in both methods also showed peaks indicating the presence of γ -alumina phase. However, for Ni-Zn by co-precipitation method, the search and match system showed the presence of calcium aluminium oxide chloride hydrate. The presence of such compound could be the reason behind the sharp and tall peaks observed in the diffractogram for Ni-Zn by co-precipitation.

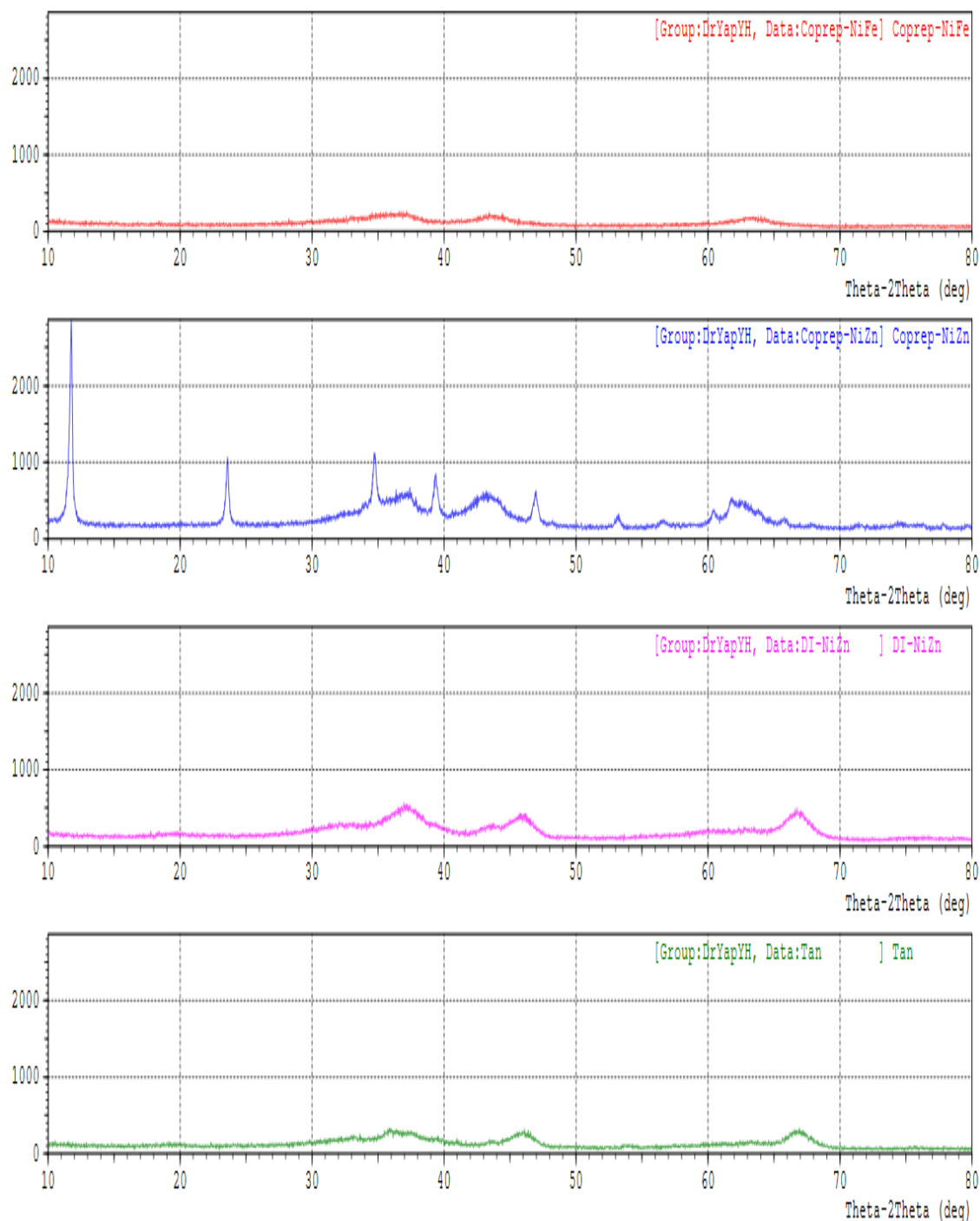


Figure 4.7: XRD Overlay diffractograms for (red) Ni-Fe by co-precipitation, (blue) Ni-Zn by co-precipitation, (pink) Ni-Fe by dry impregnation and (green) Ni-Zn by dry impregnation.

4.4.2 Temperature Programmed Reduction (TPR) Analysis

Other than the Ni-Fe/ γ -Al₂O₃ catalyst prepared by dry impregnation and co-precipitation method, three types of commercial catalyst – A, B and C were also analysed in the temperature programmed reduction analysis. The results obtained are presented in Table 4.2 with their raw data attached in Appendix J. Concurrently, TPR analysis results of Ni/ γ -Al₂O₃ and Ni-Zn/ γ -Al₂O₃ catalyst prepared by another student - Tan Wen Hsiung were also compiled for comparison in Table 4.2. The temperature at which the highest peak is located is the optimum temperature for reduction while peak at a higher temperature indicates a lower catalyst activity as more energy is required to effectively reduce the metal oxides into active metals.

Table 4.2: Optimum reduction temperature and amount of hydrogen gas adsorbed from TPR analysis.

	Dry Impregnation		Co-Precipitation		Commercial Catalyst	
	T	Gas Adsorbed ($\mu\text{mol/g}$)	T	Gas Adsorbed ($\mu\text{mol/g}$)	T	Gas Adsorbed ($\mu\text{mol/g}$)
Ni-Fe	449°C	1475.95	396°C	10681.23	-	-
Ni-Zn	496°C	634.98	540°C	2709.11	-	-
Ni	-	-	460°C	4427.23	-	-
A	-	-	-	-	386°C	6791.36
B	-	-	-	-	389°C	4483.80
C	-	-	-	-	395°C	7587.76

According to Table 4.2, the Ni-Fe/ γ -alumina catalyst prepared by dry impregnation has higher reduction temperature than the one prepared by co-precipitation. This implies that the reducibility of Ni-Fe/ γ -alumina catalyst from co-precipitation method is higher and its reaction could be carried out at lower temperature as the catalyst could be activated at a lower temperature without further heating. The results obtained are in accordance with Broecker *et al.* (1975) which used reduction temperature of 400°C for catalyst from co-precipitation method and Vogelaar *et. al.* (2010) which used 450 °C for reduction of catalyst from dry-impregnation method.

Nevertheless, the optimum reduction temperature for Ni-Zn/ γ -alumina catalyst shows opposing results. The Ni-Zn/ γ -alumina catalyst prepared by dry impregnation has lower optimum reduction temperature and thus higher reducibility than the one prepared by co-precipitation. Besides that, the Ni-Fe catalyst prepared by co-precipitation showed lower reduction temperature than the mono-metallic nickel catalyst prepared similarly. This shows that the extra presence of iron could possibly reduce the reduction temperature of the nickel catalyst.

Meanwhile, among the commercial nickel catalysts analysed, catalyst C showed the highest reduction temperature with lowest reducibility followed by catalyst B and catalyst A. When compared between synthesised catalysts and commercial ones, commercial catalysts showed higher reducibility with catalyst having the highest reducibility and lowest reduction temperature.

Besides that, the amount of hydrogen gas adsorbed serves as an indication of the relative abundance of reducible metals loaded on the catalysts. Based on Table 4.2 and height of peaks in Figure 4.8, the hydrogen gas adsorbed on Ni-Fe catalyst (red line) prepared by dry impregnation method is significantly less than the one prepared by co-precipitation method (purple line). This trend is also seen on Ni-Zn catalyst but with lower value and could be attributed to the higher metal loading in co-precipitation method. Among all the catalysts tested, amount of gas adsorbed in Ni-Fe catalyst by co-precipitation method is the highest among all the catalysts tested.

On the other hand, the TPR graphs for Ni-Fe from both dry impregnation and co-precipitation methods are compared in Figure 4.9. Both synthesis methods recorded highest peak in the temperature range of 400°C to 450°C. This result is observed to be in accordance with the TPR peaks of pure nickel catalyst at 400°C to 500°C by Mile (1990), Gamas (1997) and He *et. al.* (2015). Reports by Delahov *et. al.* (2004) and Centi *et. al.* (2000) showed that TPR peaks of pure iron catalyst were detected at around 400°C as well. Based on these literature findings, it could be deduced that the single but broad peak detected in Figure 4.9 is due to reduction of combined Ni and Fe.

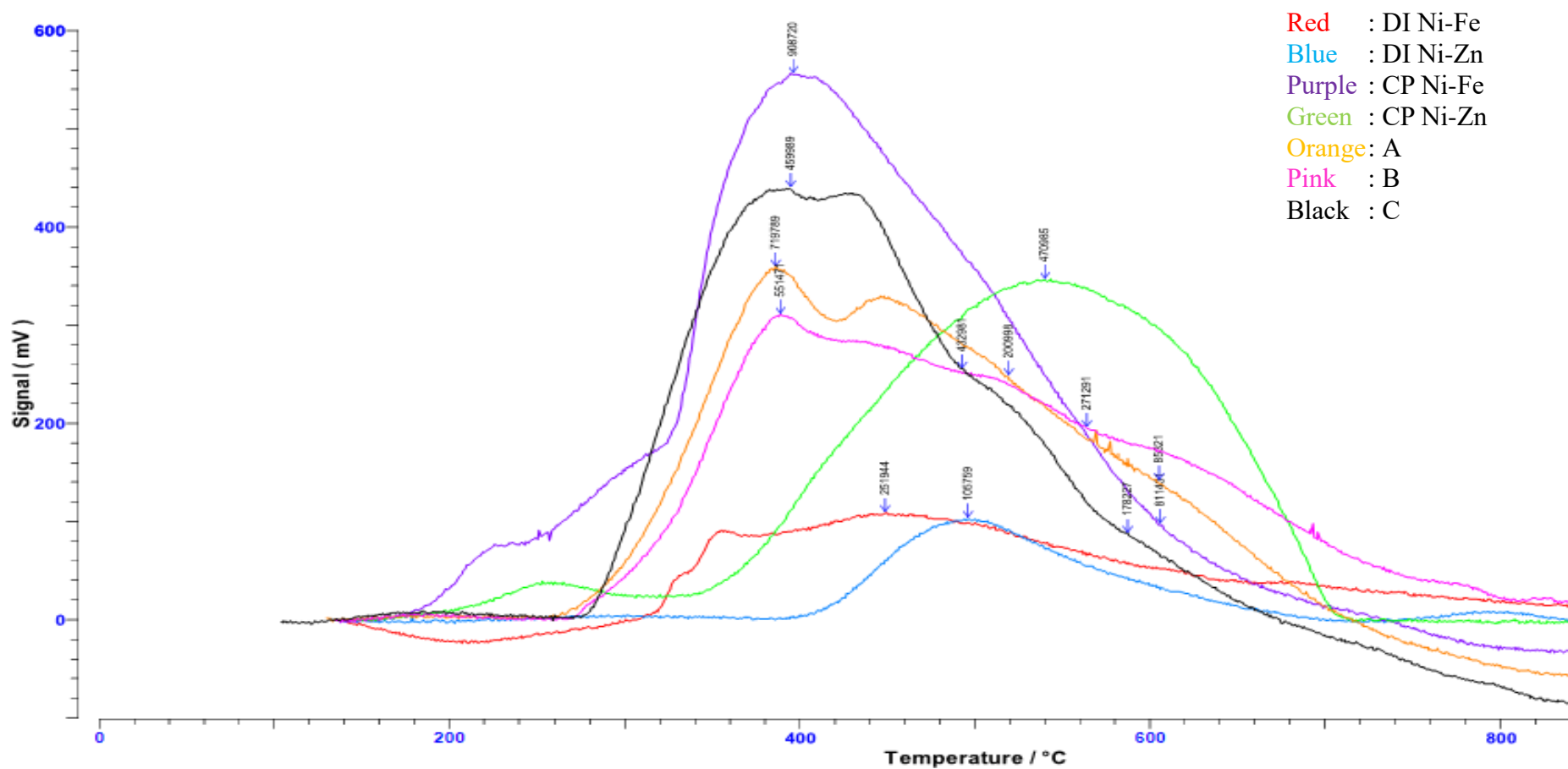


Figure 4.8: TPR Chromatogram of Synthesised and Commercial Catalysts.

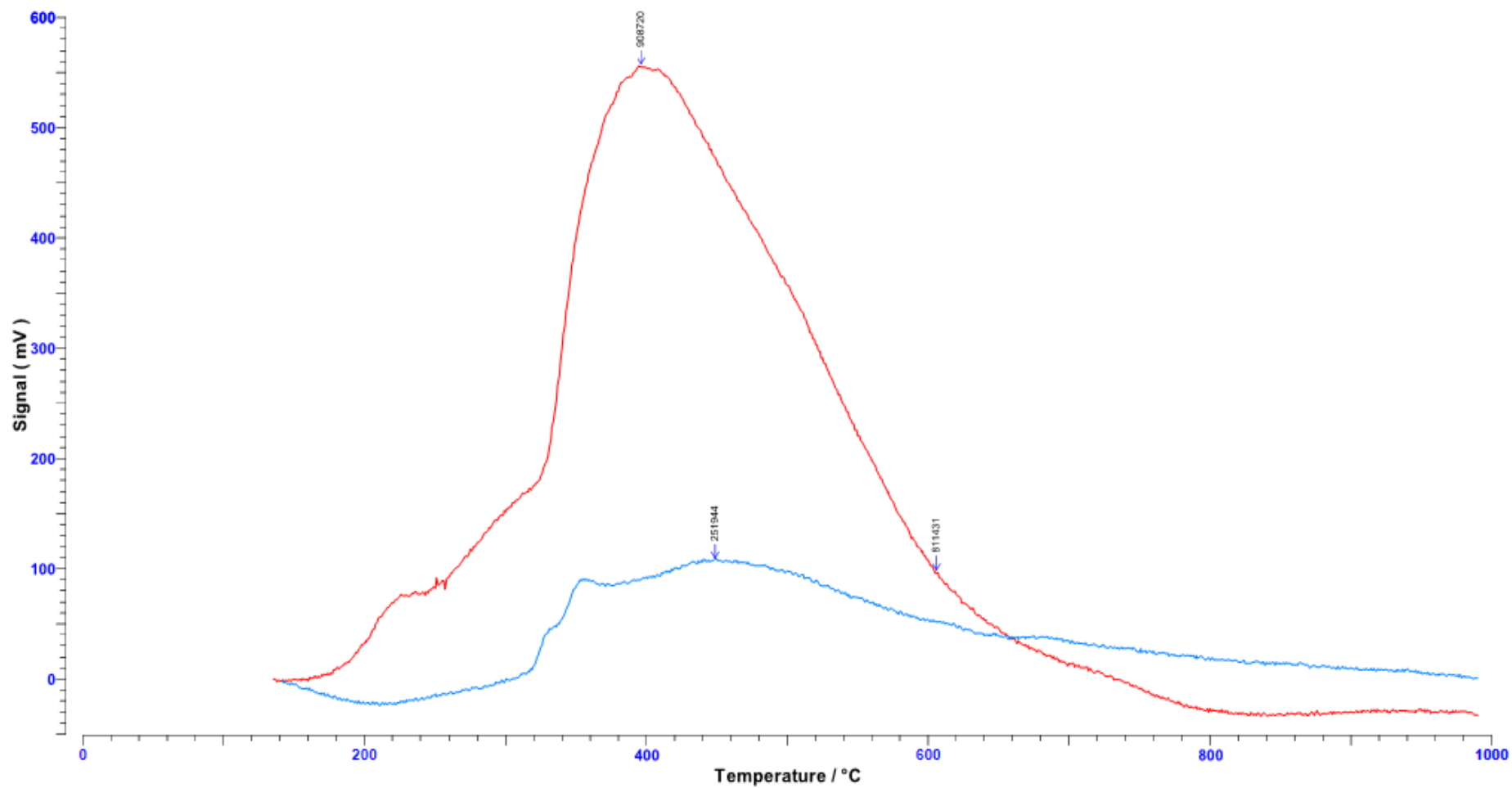


Figure 4.9: TPR chromatogram of Ni-Fe catalysts by co-precipitation method (red line) and dry impregnation method (blue line).

4.4.3 Pulse Chemisorption Analysis

The catalysts were subjected to pulse chemisorption analysis in order to investigate their metal dispersion, metal surface area and average metal particle size. The TPDRO returned the amount of gas adsorbed on the catalyst after ten pulses of 5.47% hydrogen in nitrogen gas. The amount of gas chemisorbed on the catalyst is a direct indication of the amount of active metal on the catalyst. Therefore, the readings were utilised in the calculation for metal dispersion, metal surface area and average metal particle size which are presented in detailed in Appendix H. Summary of the calculation results are shown in Table 4.3 below.

Table 4.3: Calculation Results for Pulse Chemisorption

Type	Amount of Gas Adsorbed ($\mu\text{mol/g}$ catalyst)	Amount of Gas Adsorbed ($\mu\text{mol/g}$ metal)	Dispersion (%)	Metal surface area (m^2/g)	Average Ni particle size (nm)	Average Fe or Zn particle size (nm)
DI Ni-Fe	14.42	64.06	0.74	1.26	235.95	275.20
CP Ni-Fe	120.69	163.95	1.87	10.67	111.45	89.96
DI Ni-Zn	7.52	39.38	0.49	0.60	363.33	633.35
CP Ni-Zn	124.00	152.50	1.88	9.98	91.08	170.05
CP Ni	17.66	76.78	0.91	1.48	103.16	-
A	81.29	102.87	1.21	6.83	78.02	-
B	66.55	89.76	1.05	5.59	89.41	-
C	46.03	124.59	1.46	3.87	64.41	-

As the catalysts listed above have varying metal loadings, it is unjustifiable to compare the amount of gas adsorbed based on unit mass of catalyst. In order to eliminate the effect of metal loading on the gas adsorption of each type of catalyst, the amount of gas adsorbed per unit mass of metal loading was calculated and shown in Table 4.3. This would put the catalysts on the same ground during comparison of

metal activity on each catalyst. According to the results obtained, catalysts prepared by co-precipitation method have the highest amount of gas adsorbed per mass of metals loaded, indicating higher metal activity than the rest. This could be due to their more dispersed metal phase which enables more active surface to be exposed for gas adsorption.

Based on results in Table 4.3, catalysts synthesised by co-precipitation achieve notably higher metal dispersion and larger metal surface area compared to those synthesised by dry impregnation. This trend is consistent for both Ni-Fe and Ni-Zn catalysts. The higher metal dispersion resulting from co-precipitation method is due to the simultaneous nucleation and precipitation of metals phase with the alumina support phase which promote the dispersion of the metals over the support. On the contrary, in dry-impregnation method, the alumina pellets surfaces are more unlikely to uniformly adsorb the metal phase due to varying strength of surface charges.

Meanwhile, the larger metal surface area for catalyst prepared by co-precipitation method is attributed to the higher metal loading and hence increases the number of metal surface atoms and their effective areas. Moreover, small metal particle size could also result in larger metal surface area. This could be seen in Table 4.3 where catalysts prepared from co-precipitation method show larger surface area also have smaller average particle size compared to those from dry-impregnation method. According to Perego (1997), particle size of catalyst from co-precipitation method is expected to be small. This is because the carbonate salts of transition metals have very low solubility, enabling achievement of very high supersaturation during precipitation and hence smaller particle size.

One peculiarity from the pulse chemisorption study is, the relatively large particle sizes obtained for all the catalysts samples (synthesised and commercial). Literature findings showed that the particle size for nickel hydrogenation catalyst is about 3 to 9 nm (Bouwmann *et. al.*, 2014) or 2 to 8 nm (Coenen, 1991). The result deviation could be due to insufficient reduction of the catalyst prior to pulse chemisorption analysis. Reduction was carried out in-situ of the TPDRO equipment with pre-set configuration of 400 °C for 60 minutes and gas flow rate of 20

cm³/minute. The reduction temperature was not high enough and the duration was also insufficient for complete reduction. The lack of reduced metal surface in due course led to the larger particle size compared to the findings by other researchers. Nevertheless, this is a systematic error as all of the samples were analysed under the same condition. Hence, the relative comparisons between the catalysts are still reasonably valid.

Generally, catalysts with high dispersion, large surface area and small particle size are most desirable as these characteristics show that the catalysts possess a lot metal sites that are active for reaction and accessible by reactants. By putting catalysts from the two different synthesis methods in comparison, catalyst from co-precipitation method is preferred as it fared better in all the criteria mentioned. Besides that, it was also observed that the addition of iron or zinc in the bimetallic catalysts (Ni-Fe and Ni-Zn) prepared from co-precipitation method resulted in higher dispersion, higher metal surface area and higher amount of gas adsorbed per gram of metal loaded than the mono-metallic nickel catalyst. This showed that the addition of extra metal phase (iron or zinc) could help to enhance the surface properties of nickel catalyst, giving more desirable characteristics without changing the synthesis method.

Among all the commercial catalysts, catalyst C has the best characteristic as it possesses the highest dispersion and smallest particle size with some compromise on its surface area. Besides that, all of the commercial catalysts showed smaller particle size as compared to the synthesised catalysts. However, it is noted that catalysts from co-precipitation method recorded comparable metal dispersion and also larger metal surface area than the commercial catalyst. This shows that there are more active metal sites on the catalyst by co-precipitation than the commercial catalysts, possibly allowing more catalytic activity.

4.4.4 Scanning Electron Microscopy with Energy Dispersive X-ray Spectroscopy (SEM-EDX) Analysis

The surface morphology of the synthesised Ni-Fe catalysts was observed using SEM while their surface composition were analysed by employing EDX analysis. The SEM image of Ni-Fe catalyst prepared by dry impregnation is shown in Figure 4.10 in a pellet form while Figure 4.11 clearly illustrates that the impregnated pellet surface is rough and uneven.

The results from EDX analysis are shown in Table 4.4 with the raw data attached in Appendix J. The elemental composition results in terms of weight percent are the average value from readings taken at three different spots on the same sample. Results in Table 4.4 show the presence of elements making up alumina and also total metal loading of 21.8 wt% which is almost similar to the calculation made during preparation in Section 3.4.2.

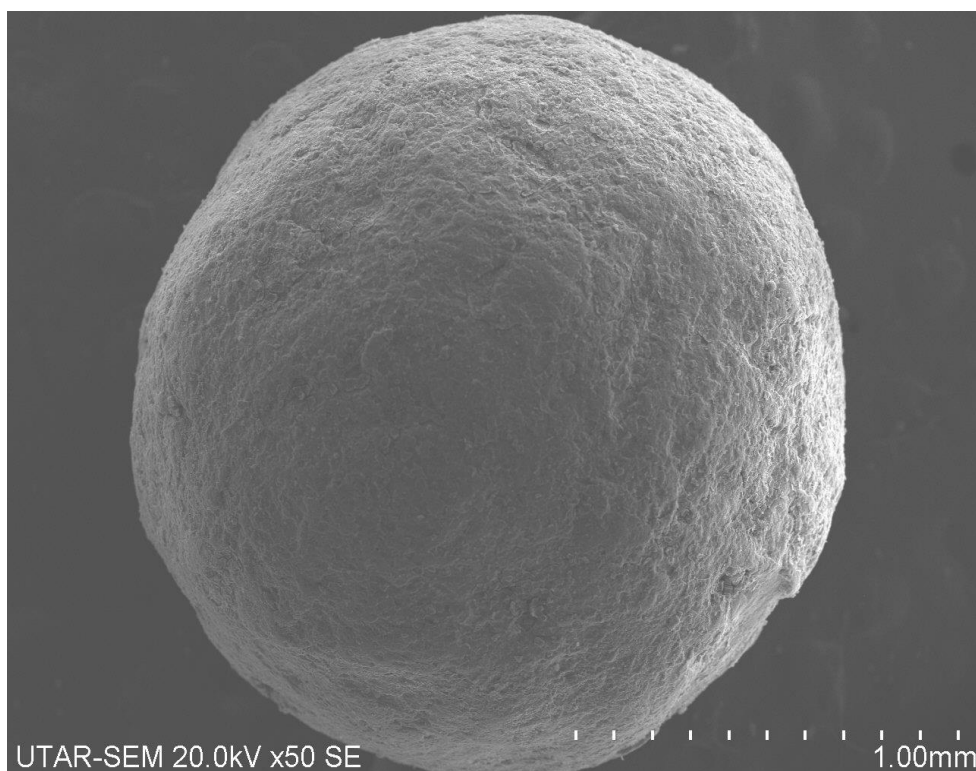


Figure 4.10: SEM image of Ni-Fe catalyst by dry impregnation method (magnification x50).

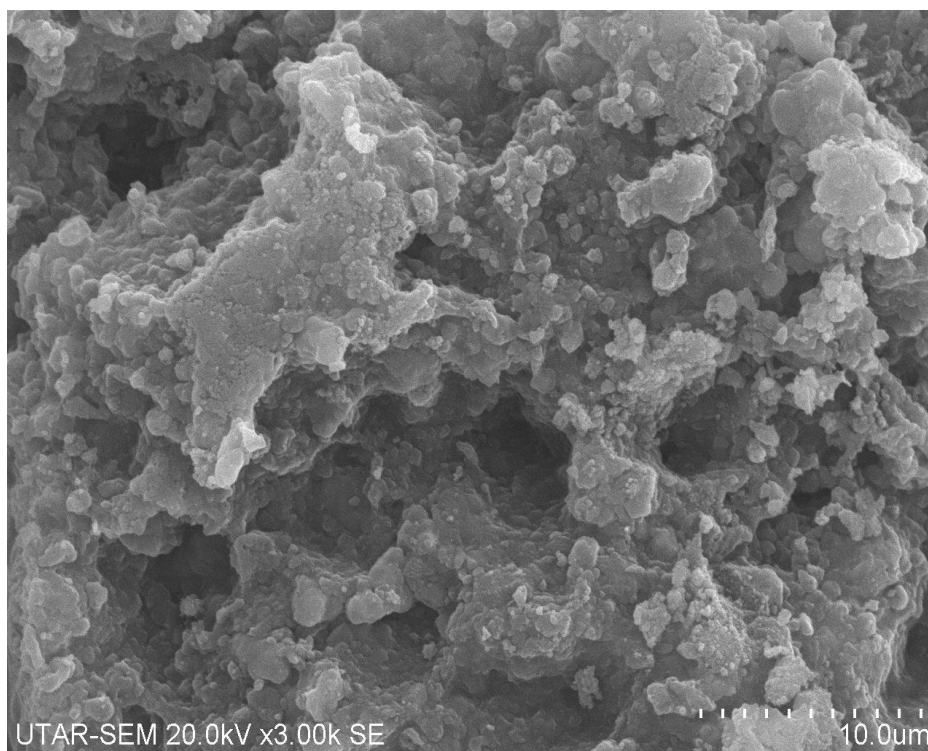


Figure 4.11: SEM image of Ni-Fe catalyst by dry impregnation method (magnification x3000).

Table 4.4: EDX elemental composition results of Ni-Fe/ γ -Al₂O₃ catalyst by dry impregnation method.

Element	Average	
	Wt%	At%
C	0.26	0.53
O	25.86	40.76
Al	51.07	48.54
Fe	9.01	4.11
Ni	13.80	6.06

Meanwhile, the SEM image of Ni-Fe/ γ -Al₂O₃ catalyst prepared by co-precipitation method is shown in Figure 4.12. Like the catalyst prepared by dry impregnation, the co-precipitated catalyst also shows a rough and uneven surface morphology. As for its surface elemental composition, the average from three spots were taken as well and tabulated in Table 4.5 below. The EDX results in Table 4.5

show that about 74.5 wt% of metals was successfully loaded onto the co-precipitated catalyst. The SEM-EDX results for Ni-Zn/ γ -Al₂O₃ catalyst and commercial catalysts are also presented in Table 4.6 for comparison.

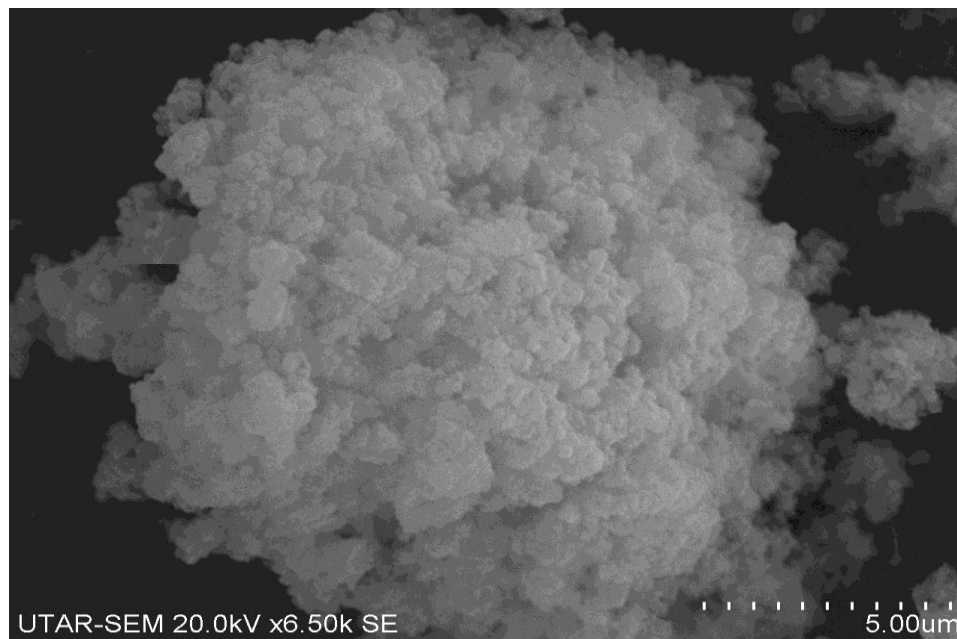
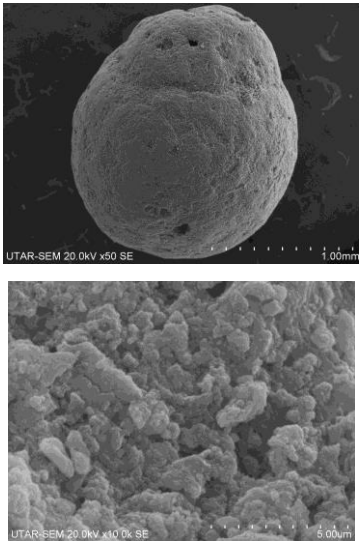
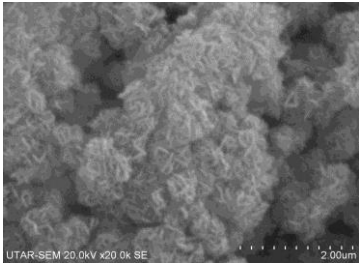

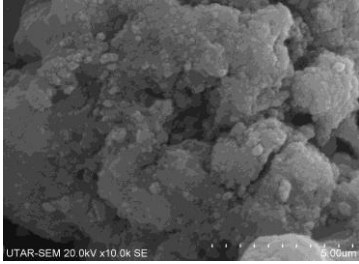


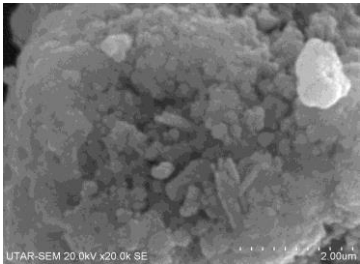
Figure 4.12: SEM image of Ni-Fe/ γ -Al₂O₃ catalyst by co-precipitation method (magnification x6500).

Table 4.5: EDX elemental composition results of Ni-Fe/ γ -Al₂O₃ catalyst by co-precipitation method.

Element	Average	
	Wt%	At%
O	19.53	44.40
Al	6.00	8.09
Fe	40.77	26.60
Ni	33.70	20.91

Table 4.6: SEM-EDX Results for Other Catalysts.

Catalyst Types	SEM Image	EDX Results																				
Ni-Zn by dry impregnation method		<table border="1"> <thead> <tr> <th rowspan="2">Element</th> <th colspan="2">Average</th> </tr> <tr> <th>Wt%</th> <th>At%</th> </tr> </thead> <tbody> <tr> <td>O</td> <td>33.88</td> <td>50.69</td> </tr> <tr> <td>Al</td> <td>47.33</td> <td>42.00</td> </tr> <tr> <td>Ni</td> <td>10.11</td> <td>4.12</td> </tr> <tr> <td>Zn</td> <td>8.69</td> <td>3.19</td> </tr> </tbody> </table>	Element	Average		Wt%	At%	O	33.88	50.69	Al	47.33	42.00	Ni	10.11	4.12	Zn	8.69	3.19			
Element	Average																					
	Wt%	At%																				
O	33.88	50.69																				
Al	47.33	42.00																				
Ni	10.11	4.12																				
Zn	8.69	3.19																				
Ni-Zn by co-precipitation method		<table border="1"> <thead> <tr> <th rowspan="2">Element</th> <th colspan="2">Average</th> </tr> <tr> <th>Wt%</th> <th>At%</th> </tr> </thead> <tbody> <tr> <td>C</td> <td>0.17</td> <td>0.59</td> </tr> <tr> <td>O</td> <td>13.82</td> <td>36.25</td> </tr> <tr> <td>Al</td> <td>4.99</td> <td>7.76</td> </tr> <tr> <td>Ni</td> <td>44.32</td> <td>31.77</td> </tr> <tr> <td>Zn</td> <td>36.70</td> <td>23.63</td> </tr> </tbody> </table>	Element	Average		Wt%	At%	C	0.17	0.59	O	13.82	36.25	Al	4.99	7.76	Ni	44.32	31.77	Zn	36.70	23.63
Element	Average																					
	Wt%	At%																				
C	0.17	0.59																				
O	13.82	36.25																				
Al	4.99	7.76																				
Ni	44.32	31.77																				
Zn	36.70	23.63																				
A		<table border="1"> <thead> <tr> <th rowspan="2">Element</th> <th colspan="2">Average</th> </tr> <tr> <th>Wt%</th> <th>At%</th> </tr> </thead> <tbody> <tr> <td>C</td> <td>0.54</td> <td>1.78</td> </tr> <tr> <td>O</td> <td>14.33</td> <td>35.62</td> </tr> <tr> <td>Mg</td> <td>1.19</td> <td>1.94</td> </tr> <tr> <td>Si</td> <td>5.67</td> <td>8.04</td> </tr> <tr> <td>Ni</td> <td>78.45</td> <td>53.22</td> </tr> </tbody> </table>	Element	Average		Wt%	At%	C	0.54	1.78	O	14.33	35.62	Mg	1.19	1.94	Si	5.67	8.04	Ni	78.45	53.22
Element	Average																					
	Wt%	At%																				
C	0.54	1.78																				
O	14.33	35.62																				
Mg	1.19	1.94																				
Si	5.67	8.04																				
Ni	78.45	53.22																				
B		<table border="1"> <thead> <tr> <th rowspan="2">Element</th> <th colspan="2">Average</th> </tr> <tr> <th>Wt%</th> <th>At%</th> </tr> </thead> <tbody> <tr> <td>O</td> <td>16.46</td> <td>39.33</td> </tr> <tr> <td>Mg</td> <td>1.22</td> <td>1.91</td> </tr> <tr> <td>Si</td> <td>6.80</td> <td>9.25</td> </tr> <tr> <td>Ca</td> <td>0.90</td> <td>0.87</td> </tr> <tr> <td>Ni</td> <td>74.61</td> <td>48.64</td> </tr> </tbody> </table>	Element	Average		Wt%	At%	O	16.46	39.33	Mg	1.22	1.91	Si	6.80	9.25	Ca	0.90	0.87	Ni	74.61	48.64
Element	Average																					
	Wt%	At%																				
O	16.46	39.33																				
Mg	1.22	1.91																				
Si	6.80	9.25																				
Ca	0.90	0.87																				
Ni	74.61	48.64																				

C		Average		
		Element	Wt%	At%
		O	28.76	47.17
		Na	1.19	1.35
		Mg	0.86	0.95
		Al	5.22	5.08
		Si	31.04	29.16
		K	3.15	2.13
		Ni	29.78	14.15

CHAPTER 5

CONCLUSION AND RECOMMENDATIONS

5.1 Conclusion

In this project, Ni-Fe/ γ -Al₂O₃ bimetallic catalysts have been synthesised and characterised. The project objectives have been achieved where:

1. Ni-Fe/ γ -Al₂O₃ catalysts have been prepared by charge enhanced dry impregnation (CEDI), dry impregnation (DI) and co-precipitation methods.
 - a. While employing CEDI, it was found that the presence of large amount of hydroxyl ions from the alkali (NaOH) added to deprotonate the support surface would react with the cationic metal precursors to form insoluble metal hydroxides. Therefore, it was not possible to employ CEDI to synthesise Ni-Fe/ γ -Al₂O₃ catalysts.
 - b. Catalysts synthesised by conventional dry impregnation were dark-brown pellets that showed static charge interaction with the walls of the container. Meanwhile, catalysts synthesised by co-precipitation were fine powders in dark brown colour.
2. The synthesised catalysts and three commercial catalysts were characterised by XRD, TPR, Pulse Chemisorption and SEM-EDX analyses.

3. It was found that catalysts prepared by co-precipitation method showed more desirable characteristics such as higher metal loading, higher dispersions, smaller particle size and higher reducibility compared to catalysts prepared by dry impregnation method. This was observed for both of the Ni-Zn/ γ -Al₂O₃ and Ni-Fe/ γ -Al₂O₃ catalysts.
4. When compared to Ni-Zn/ γ -Al₂O₃ catalysts, the Ni-Fe/ γ -Al₂O₃ catalysts showed much lower crystallinity due to its broad and short peaks in XRD chromatograms. In terms of metal loading, dispersions, and reducibility, both of the bimetallic catalysts from co-precipitation method showed comparable characteristics. Meanwhile for dry impregnation method, Ni-Fe/ γ -Al₂O₃ catalysts showed higher readings than Ni-Zn/ γ -Al₂O₃ catalysts.
5. In comparison with commercial catalysts, the catalysts prepared by co-precipitation (both Ni-Zn and Ni-Fe) fared better in terms of metal dispersion and metal surface area. Despite having higher reduction temperature and metal particle size, the synthesised catalysts were comparable to the commercial catalysts.

5.2 Recommendations

While this project covered much ground, there are significant gaps that have to be filled in order to determine the suitability of the synthesised catalysts for the hydrogenation of fatty acids. Subsequent work in this topic can include:

- Employing anionic metal precursor ions for CEDI instead of cationic metal precursor (such as nickel nitrate) for charging of support surface. In the case of nickel, complexes such as lanthanum nickelate are possible candidates.
- Testing the Ni-Fe/ γ -Al₂O₃ catalysts with hydrogenation reaction as there is no better way to determine the suitability than to test it in real process.

- Other catalyst characterisation techniques such as Transmission Electron Microscope (TEM) and X-ray Photoelectron Spectroscopy (XPS) can be employed to study the catalysts as they allow the determination of metal particle size and the state of the metal phase (e.g. homogeneous alloy or core-shell structure).

REFERENCES

- Adkins H. (1930). The Use of Nickel as a Catalyst for Hydrogenation. *A Communication from The Laboratory of Organic Chemistry of The University of Wisconsin* vol.52
- Aylesworth, R.D. (1955). Applications for Fatty Acids. *Fatty Acids for Chemical Specialties* pp.142
- Bartholomew, C. H. and Farrauto, R. J. (1976). Chemistry of Nickel-Alumina Catalysts. *Journal of Catalysis*, 45, 41-53
- Beers, A. E. W. (2007). Low Trans Hydrogenation of Edible Oil. *Lipid Technology*, 19(3)
- Behr, A. *et. al.* (2008). Catalytic Processes for the Technical Use of Natural Fats and Oils. *Chem. Eng. Technol.* 2008, 31, No. 5, 700–714
- Belkacemi, K. and Hamoudi, S. (2009). Low Trans and Saturated Vegetable Oil Hydrogenation over Nanostructured Pd/Silica Catalysts: Process Parameters and Mass-Transfer Features Effects. *Ind. Eng. Chem. Res.* 2009, 48, 1081–1089
- Bergeret, G. *et. al.* (2008). Particle Size and Dispersion Measurements. In Ertl *et. al.*, *Handbook of Heterogeneous Catalyst* pp.738
- Black, H.C. (1955). Basic Chemistry of Fatty Acids. *Fatty Acids for Chemical Specialties* pp.131
- Bouwman *et. al.* (2014). Nickel Hydrogenation Catalyst. Patent Application Publication US 2014/0256972 A1
- Broecker *et. al.* (1973). Nickel-containing Hydrogenation Catalysts for the Selective Hydrogenation of Fats and Oils. Patent Application Publication US 3896053
- Campanati, M. *et. al.* (2003). Fundamentals in the preparation of heterogeneous catalysts. *Catalysis Today*, 77, 299–314

- Cao, C.J. *et al.* (2014). Selective adsorption of palladium complex for carbon-supported Pd/Mo electrocatalyst by the charge enhanced dry impregnation method. *Journal of Power Sources* 272 (2014) 1030-1036
- Centi C. *et al.* (2000). SO₂ resistant Fe/ZSM-5 catalysts for the conversion of nitrogen oxides. *Studies in Surface Science and Catalysis* 130
- Chen I. (1988). Reduction of Nickel-Alumina Catalysts. *Ind. Eng. Chem. Res.*, 27(3)
- Coenen, J. W. E. (1986). Catalytic Hydrogenation of Fatty Oils. *Industrial Engineering Chemistry Fundamental* 25(1)
- Combs, D.L. (1985). Processing for Industrial Fatty Acids. *The Journal of American Oil Chemist's Society*, 62, 02
- Delahav, G. *et al.* (2004). Selective Catalytic Reduction of NO by NH₃ on Fe-ZSM-5 Elaborated From Different Methods. *Studies in Surface Science and Catalysis*, Volume 154. Elsevier B.V.
- Enthaler, S. *et al.* (2008). Sustainable Catalysis with Iron: From Rust to a Rising Star? *Angewandte Chemie Int. Ed.* 2008, 47, 3317 – 3321
- Epinosa, L. *et al.* (2008). Effect of the Nickel Precursor on the Impregnation and Drying of γ -Al₂O₃ Catalyst Bodies: A UV-vis and IR Microspectroscopic Study. *Journal of Physical Chemistry C* 2008, 112, 7201-7209
- Ertl, G. *et al.* (1999). Precipitation and Co-precipitation. In *Preparation of Solid Catalyst*. Wiley-VCH.
- Gamas, E.D. and Schifter, I. (1997). Influence of the Support on the Deactivation of Nickel Zeolite Catalysts. *Catalyst Deactivation*. Elsevier Science B.V.
- Gervajio, C.G. (2005). Fatty Acids and Derivatives from Coconut Oil. In *Bailey's Industrial Oil and Fat Products*. Wiley-Interscience.
- Geus J.W. (2007). Production of Supported Catalysts by Impregnation and (Viscous) Drying. In Regalbuto, J. R. (ed.) *Catalyst Preparation*. CRC Press, Florida
- Gutsche, B. *et al.* (2008). Heterogeneous Catalysis in Oleochemistry. *Handbook of Heterogeneous Catalysis*. Wiley-VCH Verlag GmbH & Co
- Haber, J. *et al.* (2005). Manual of Methods and Procedures for Catalyst Characterization. *Pure & Applied Chemistry*, Vol. 67, Nos 8/9, pp. 1257-1306
- Hao, X. *et al.* (2003). A further simplification of the revised physical adsorption (RPA) model. *Journal of Colloid and Interface Science* 267 (2003) 259–264

- Harper, M.J. (2000). Raney Iron Catalyst and a Process for Hydrogenating Organic Compounds Using Said Catalyst. Patent Application Publication US 6087296
- Hastert, R.C. (1979). Hydrogenation of Fatty Acids. *The Journal of American Oil Chemist's Society*, 56
- He, S.F. *et. al.* (2015). Ni/SiO₂ Catalyst Prepared with Nickel Nitrate Precursor for Combination of CO₂ Reforming and Partial Oxidation of Methane: Characterization and Deactivation Mechanism Investigation. *Journal of Nanomaterials*, Volume 2015, Article ID 659402
- Hoffman, G. (1989). The Chemistry and Technology of Edible Oils and Fats and Their High Fat Products. Academic Press.
- Huang Y. J. and Schwarz, J. A. (1987). The Effect of Catalyst Preparation on Catalytic Activity: III. The Catalytic Activity of Ni/Al₂O₃ Catalysts Prepared by Incipient Wetness. *Applied Catalysis*, 32, 45-57
- Hudson, R. *et. al.* (2013). Highly Efficient Iron(0) Nanoparticle-Catalyzed Hydrogenation in Water in Flow. *The Royal Society of Chemistry*
- Hwang, S. J. *et. al.* (2013). Supported Core@Shell Electrocatalysts for Fuel Cells: Close Encounter with Reality. *Scientific Reports*, 3, 1309
- Johanes, B.H. *et. al.* (2011). Hydrogenation of fatty acids using a promoted supported nickel catalyst. *European Patent Application* EP 2 380 953 A1
- Jang *et. al.* (2005). Hydrogenation for Low Trans and High Conjugated Fatty Acids. *Comprehensive reviews in Food Science and Food Safety*.
- Jung (1982). CO Hydrogenation over Well-dispersed Carbon Supported Iron Catalyst. *Journal of Catalysis* 75, 416-422
- Lee, M.D. *et. al.* (1989). Catalytic Behaviour and Phase Composition Change of Fe Catalyst in Hydrogenation of Carbon Dioxide. *Journal of Chemical Engineering of Japan*
- Lee, M.D. *et. al.* (1989). Hydrogenation of Carbon Dioxide on Unpromoted and Potassium Promoted Iron Catalyst. *Chemical Society of Japan*, 62, 2756-2758
- Li G.H. *et. al.* (2005). Comparison of Reducibility and Stability of Alumina-Supported Ni Catalysts Prepared by Impregnation and Co-Precipitation. *Applied Catalysis A: General* 301 (2006) 16–24

- Li W.D. *et al.* (1994). Theoretical Prediction and Experimental Validation of The Egg-Shell Distribution of Ni for Supported Ni/ Al₂O₃ Catalysts. *Chemical Engineering Science*, 49(24A). pp, 4889-4895
- Lok M. (2009). Coprecipitation. In De Jong K.P. (ed.) *Synthesis of Solid Catalyst*. Wiley-VCH, Weinheim
- Louis, C. (2007). Deposition-Precipitation Synthesis of Supported Metal Catalysts. In Regalbuto, J. R. (ed.) *Catalyst Preparation*. CRC Press, Florida
- Lowell, S. *et al.* (2004). Characterization of Porous Solids and Powder: Surface Area, Pore Size and Density. Kluwer Academic Publisher, Netherlands
- Marceau E. *et al.* (2009). Impregnation and Drying. In De Jong K.P. (ed.) *Synthesis of Solid Catalyst*. Wiley-VCH, Weinheim
- Michaelis, D.J. (2008). Iron as Powerful Catalyst for Transition Metal-Catalysed Reaction.
- Mile, B. *et al.* (1990). TPR Studies of the Effects of Preparation Conditions on Supported Nickel Catalysts. *Journal of Molecular Catalysis*, 62 (1990) 179-198
- Montes, M. *et al.* (1984). Influence of Metal-Support Interactions on the Dispersion, Distribution, Reducibility and Catalytic Activity of Ni/SiO₂ Catalysts. *Applied Catalysis*, 12, 309-330
- Nakai, K. *et al.* (2003). Pulse chemisorption measurement. *BEL-CAT Application note*, CAT-APP-002
- Perego C. (1997). Catalyst Preparation Methods. *Catalysis Today* 34 (1997) 281-305
- Persson *et al.* (2006). Characterisation and Microstructure of Pd and Bimetallic Pd–Pt Catalysts During Methane Oxidation. *Journal of Catalysis*. 245, 401–414
- Rozita, Y. *et al.* (2010). An investigation of commercial gamma-Al₂O₃ nanoparticles. *Journal of Physics: Conference Series* 241 (2010) 012096
- Ruston, N.A. (1952). Commercial Uses of Fatty Acids. *The Journal of American Oil Chemist's Society*, November.
- Salimon, J. *et al.* (2011). Hydrolysis optimization and characterization study of preparing fatty acids from *Jatropha curcas* seed oil. *Chemistry Central Journal* 2011, 5:67
- Savchenko, V. I. and Makayan, I. A. (1999). Palladium Catalyst for the Production of Pure Margarine. *Platinum Metals Rev.*, 43, (2)

- Scrimgeour, C. (2005). Chemistry of Fatty Acids. In *Bailey's Industrial Oil and Fat Products*. Wiley-Interscience.
- Simpson H.D. (1995). Hydroprocessing catalytic composition and the preparation and use thereof. European Patent Specification Publication 0 349 223 B1
- Subramani V. (2006). Synthesis of alumina supported nickel nanoparticle catalysts and evaluation of nickel metal dispersions by temperature programmed desorption. *Solid State Ionics* 177 (2006) 803–811
- Suyenty, E. *et. al.* (2007). Catalyst in Basic Oleochemicals. *Bulletin of Chemical Reaction Engineering & Catalysis*, 2(2-3), 2007, 22-31
- Tike, M.A. (2006). Kinetics of Hydrogenation of Palm Stearin Fatty Acids over Ru/Al₂O₃ in Presence of Small Quantity of Water. *Indian Journal of Chemical Technology*, 14, 52-63
- Toebes, M. L. *et. al.* (2000). Synthesis of supported palladium catalysts. *Journal of Molecular Catalysis A: Chemical* 173, 75–98
- Tong, D.G. *et. al.* (2007). Effect of crystallinity on the catalytic performance of amorphous Co–B particles prepared from cobalt nitrate and potassium borohydride in the cinnamaldehyde hydrogenation. *Journal of Molecular Catalysis A: Chemical* 265 (2007) 195–204
- Trueba, M. and Trasatti, S.P. (2005). γ -Alumina as a Support for Catalysts: A Review of Fundamental Aspects. *European Journal of Inorganic Chemistry* 2005, 3393–3403
- Viet Long, N. *et. al.* (2011). Synthesis and characterization of PtePd alloy and core-shell bimetallic nanoparticles for direct methanol fuel cells (DMFCs): Enhanced electrocatalytic properties of well-shaped core-shell morphologies and nanostructures. *International Journal of Hydrogen Energy*, 36, 8478-8491
- Vogelaar B.M. *et. al.* (2010). Stability of Metal Nanoparticles Formed During Reduction of Alumina Supported Nickel and Cobalt Catalysts. *Catalysis Today* 163 (2011) 20–26
- Weiting Yu *et. al.* (2012). Review of Pt-based Bimetallic Catalyst: From Model Surfaces to Supported Catalyst. *Chemical Reviews*.
- Wittcoff, H. (1955). Relationship of Use of Fatty Acids to their Properties and Analytical Method. *Fatty Acids for Chemical Specialties* pp.133
- Zhu *et. al.* (2013). Charge-Enhanced Dry Impregnation: A Simple Way to Improve the Preparation of Supported Metal Catalysts. *ACS Catalysis* 3, 625–630

Zinzalian, G. (1955). Storage and Handling of Fatty Acids. *Fatty Acids for Chemical Specialties* pp.141

APPENDICES

APPENDIX A: Surface Loading Calculation

Surface loading is calculated by the following formula:

$$SL \left(\frac{m^2}{L} \right) = \frac{m \text{ (g)} \times A \left(\frac{m^2}{g} \right)}{V \text{ (L)}}$$

where m = mass of oxide support (g)

A = specific surface area of oxide support (m^2/g)

V = volume of impregnating solution (L)

The specific surface area of oxide support was given to be $300 \text{ m}^2/g$ while the mass of oxide support was fixed at 0.05g . Other surface loadings were obtained by only varying the volume of impregnating solution.

Sample Calculation

$$SL = \frac{0.05 \text{ g} \times 300 \frac{m^2}{g}}{0.1 \text{ L}}$$

$$SL = 150 \frac{m^2}{L}$$

Table A.1: Surface Loadings Calculation.

m (g)	A (m^2/g)	V (L)	SL (m^2/L)
0.05	300	0.100	150
0.05	300	0.050	300
0.05	300	0.025	600

APPENDIX B: Calculation for Preparation of Catalyst by CEDI Method

Amount of metal precursors required:

Sample Calculation

$$\text{Total mass of catalyst} = 15 \text{ g}$$

$$\text{Total metal loading} = 2 \text{ wt\%}$$

$$\text{Nickel loading} = 1.025 \text{ wt\%}$$

$$\text{Iron loading} = 0.975 \text{ wt\%}$$

$$\begin{aligned} \text{Total oxide support} &= (1 - 0.02) \times 15 \\ &= 14.7 \text{ g} \end{aligned}$$

$$\text{Support pore volume} = 1 \frac{\text{cm}^3}{\text{g}}$$

$$\begin{aligned} \text{Volume of impregnating solution} &= 14.7 \text{ g} \times 1 \frac{\text{cm}^3}{\text{g}} \times \frac{1 \text{ ml}}{1 \text{ cm}^3} \\ &= 14.7 \text{ ml} \end{aligned}$$

Based on condition of equimolar metal loading,

$$\text{Mole of nickel required} = 0.002619 \text{ mol}$$

$$\text{Mole of iron required} = 0.002619 \text{ mol}$$

$$\begin{aligned} \text{Mass of Ni(NO}_3)_2 \cdot 6\text{H}_2\text{O} &= \frac{1 \text{ mol Ni(NO}_3)_2 \cdot 6\text{H}_2\text{O}}{1 \text{ mol Ni}} \times 0.002619 \text{ mol} \times 290.79 \frac{\text{g}}{\text{mol}} \\ &= 0.7616 \text{ g} \end{aligned}$$

$$\begin{aligned} \text{Mass of Fe(NO}_3)_3 \cdot 9\text{H}_2\text{O} &= \frac{1 \text{ mol Fe(NO}_3)_3 \cdot 9\text{H}_2\text{O}}{1 \text{ mol Fe}} \times 0.002619 \text{ mol} \times 404 \frac{\text{g}}{\text{mol}} \\ &= 1.058 \text{ g} \end{aligned}$$

APPENDIX C: Calculation for Preparation of Catalyst by Dry Impregnation Method

Amount of metal precursors required:

Sample Calculation

$$\text{Total mass of catalyst} = 15 \text{ g}$$

$$\text{Total metal loading} = 20 \text{ wt\%}$$

$$\text{Nickel loading} = 10.248 \text{ wt\%}$$

$$\text{Iron loading} = 9.752 \text{ wt\%}$$

$$\begin{aligned} \text{Total oxide support} &= (1 - 0.20) \times 15 \\ &= 12 \text{ g} \end{aligned}$$

$$\text{Support pore volume} = 1 \frac{\text{cm}^3}{\text{g}}$$

$$\begin{aligned} \text{Volume of impregnating solution} &= 12 \text{ g} \times 1 \frac{\text{cm}^3}{\text{g}} \times \frac{1 \text{ ml}}{1 \text{ cm}^3} \\ &= 12 \text{ ml} \end{aligned}$$

Based on condition of equimolar metal loading,

$$\text{Mole of nickel required} = 0.02619 \text{ mol}$$

$$\text{Mole of iron required} = 0.02619 \text{ mol}$$

$$\begin{aligned} \text{Mass of Ni(NO}_3)_2 \cdot 6\text{H}_2\text{O} &= \frac{1 \text{ mol Ni(NO}_3)_2 \cdot 6\text{H}_2\text{O}}{1 \text{ mol Ni}} \times 0.02619 \text{ mol} \times 290.79 \frac{\text{g}}{\text{mol}} \\ &= 7.6165 \text{ g} \end{aligned}$$

$$\begin{aligned} \text{Mass of Fe(NO}_3)_3 \cdot 9\text{H}_2\text{O} &= \frac{1 \text{ mol Fe(NO}_3)_3 \cdot 9\text{H}_2\text{O}}{1 \text{ mol Fe}} \times 0.02619 \text{ mol} \times 404 \frac{\text{g}}{\text{mol}} \\ &= 10.5817 \text{ g} \end{aligned}$$

APPENDIX D: Calculation for Preparation of Catalyst by Co-Precipitation Method

Amount of metal precursors required:

Sample calculation

$$\text{Mass of Ni(NO}_3)_2 \cdot 6\text{H}_2\text{O} = 1.5 \text{ mol} \times 290.79 \frac{\text{g}}{\text{mol}}$$

$$= 436.09 \text{ g}$$

$$\text{Scaled down mass} = 436.09 \text{ g} \div 15$$

$$= 29.08 \text{ g}$$

Solution	Chemical	Moles	MW (g/mol)	Mass (g)	Scale down factor	Scaled down mass (g)
1	Ni(NO ₃) ₂ · 6H ₂ O	1.5	290.79	436.09	15	29.079
	Fe(NO ₃) ₃ · 9H ₂ O	1.5	404.00	606.00	15	40.4000
	Al(NO ₃) ₃ · 9H ₂ O	1	375.13	375.13	15	25.0087
2	NaHCO ₃	10	84.01	840.10	15	56.0067

Volume of deionised water required:

Sample calculation

$$\text{Total moles in Solution 1} = 1.5 + 1.5 + 1$$

$$= 4 \text{ mol}$$

$$\text{Volume of water required} = 4 \text{ mol} \div 2 \text{ mol/L}$$

$$= 2 \text{ L}$$

$$\text{Scaled down volume} = 2 \text{ L} \div 15$$

$$= 0.13 \text{ L}$$

Solution	Moles	Target Concentration (mol/L)	Volume needed (L)	Scale down factor	Scaled down volume (L)	Scaled down volume (ml)
1	4	2	2	15	0.13	133.33
2	10	2	5	15	0.33	333.33

Volume of deionised water required in precipitating vessel:

Sample calculation

$$\begin{aligned}\text{Volume reduction factor of Solution 1} &= \frac{\text{Volume of Solution 1}}{\text{Volume of Solution 1 in literature}} \\ &= \frac{2 \text{ L}}{128 \text{ L}} \\ &= 0.0156\end{aligned}$$

$$\begin{aligned}\text{Volume of water required} &= \text{Volume in literature} \times \text{Volume reduction factor} \\ &= 40 \text{ L} \times 0.0156 \\ &= 0.625 \text{ L}\end{aligned}$$

$$\begin{aligned}\text{Scaled down volume of water required} &= 0.625 \text{ L} \div 15 \\ &= 0.0417 \text{ L}\end{aligned}$$

APPENDIX E: Raw Data for PZC Determination in CEDI Method

Table E.1: Raw Data for PZC Determination.

SL = 150 m²/L		SL = 300 m²/L		SL = 600 m²/L	
Initial pH	Final pH	Initial pH	Final pH	Initial pH	Final pH
2.74	2.99	3.75	4.65	4.14	7.09
5.55	6.10	5.88	5.87	6.44	6.37
6.94	6.16	6.66	6.32	7.20	7.24
7.84	8.18	7.17	6.50	8.40	7.15
9.38	7.83	8.86	6.17	9.15	7.20
10.04	8.92	9.63	6.50	9.71	7.32

APPENDIX F: Raw Data and Sample Calculation for Determination of pH for
Optimal Adsorption in CEDI

In order to get precursor solution of 20 ppm,

Mass of precursor solution added = 0.6 mg

Volume of deionised water = 30 mL

$$\begin{aligned} \text{ppm of precursor solution} &= \frac{0.6 \text{ mg}}{30 \text{ mL}} \times \frac{1000 \text{ mL}}{\text{L}} \\ &= 20 \frac{\text{mg}}{\text{L}} \text{ or } 20 \text{ ppm} \end{aligned}$$

Calculation of adsorption density based on ICP-OES results:

Sample Calculation

The adsorption density is calculated by the following formula:

$$\Gamma \left(\frac{\text{nmol}}{\text{m}^2} \right) = \frac{(C_{\text{initial}} - C_{\text{final}}) \frac{\mu\text{g}}{\text{L}} \times \frac{10^3 \text{ nmol}}{\mu\text{mol}}}{\text{SL} \left(\frac{\text{m}^2}{\text{L}} \right) \times \text{MW} \left(\frac{\mu\text{g}}{\mu\text{mol}} \right)}$$

where C_{initial} = initial concentration of impregnating solution ($\mu\text{g/L}$)

C_{final} = final concentration of impregnating solution ($\mu\text{g/L}$)

SL = surface loading of oxide support (m^2/L)

MW = molecular weight of metal ($\mu\text{g}/\mu\text{mol}$)

By using the set of data with initial pH of 6.28,

$$\begin{aligned} \Gamma \left(\frac{\mu\text{mol}}{\text{m}^2} \right) &= \frac{(7.371 - 1.6) \left(\frac{\text{mg}}{\text{L}} \right) \times 10^6 \left(\frac{\mu\text{mol}}{\text{mol}} \right)}{600 \left(\frac{\text{m}^2}{\text{L}} \right) \times 58.6934 \left(\frac{\text{g}}{\text{mol}} \right) \times 1000 \left(\frac{\text{mg}}{\text{g}} \right)} \\ &= 0.1639 \frac{\mu\text{mol}}{\text{m}^2} \end{aligned}$$

Table F.1: Adsorption Density for Nickel.

Initial		Final		Adsorption density, Γ (nmol/m²)
pH	Concentration (µg/L)	pH	Concentration (µg/L)	
1.08	10.70	1.32	11.57	-0.0247
3.11	9.13	5.22	8.64	0.0140
5.83	8.15	7.74	2.90	0.1491
6.28	7.37	7.73	1.60	0.1639
8.52	1.60	8.89	0.00	0.0455
9.65	0.00	8.63	0.00	0.0000
10.76	0.58	9.73	0.00	0.0165
11.44	0.00	10.70	0.00	0.0000
12.48	1.23	12.38	0.00	0.0348
13.14	0.00	13.12	0.00	0.0000

Table F.2: Adsorption Density for Iron.

Initial		Final		Adsorption density, Γ (nmol/m²)
pH	Concentration (µg/L)	pH	Concentration (µg/L)	
1.33	4.99	1.30	6.31	-0.0395
3.10	1.74	4.85	1.06	0.0204
5.21	4.25	7.61	0.00	0.1269
6.21	1.64	6.62	0.00	0.0491
7.10	1.01	6.80	0.00	0.0301
9.64	2.97	7.17	0.01	0.0882
10.21	2.32	9.76	1.66	0.0197
11.38	5.49	10.58	0.01	0.1637
12.53	3.42	12.47	0.01	0.1017
13.21	1.99	13.14	0.00	0.0594

APPENDIX G: Calculation of Theoretical Optimum pH for Adsorption in CEDI

Specific surface area of alumina = $300 \text{ m}^2/\text{g}$

Hydroxyl density on alumina = $8 \text{ OH}^-/\text{nm}^2$

Mass of alumina required = 14.7 g

$$\begin{aligned} \text{Moles of hydroxyls available} &= 14.7 \text{ g} \times 300 \frac{\text{m}^2}{\text{g}} \times \frac{10^{18} \text{ nm}^2}{\text{m}^2} \times 8 \frac{\text{OH}^-}{\text{nm}^2} \times \frac{\text{mol}}{6.02 \times 10^{23} \text{ atom}} \\ &= 0.0586 \text{ mol} \end{aligned}$$

To obtain same amount of hydroxide ions from NaOH solution,

Moles of hydroxides required = 0.0586 mol

Volume of impregnating solution = 0.0147 L

$$\begin{aligned} \text{Required concentration of hydroxide ions} &= \frac{0.0586 \text{ mol}}{0.0147 \text{ L}} \\ &= 3.9864 \text{ mol/L} \end{aligned}$$

$$\begin{aligned} \text{Required pOH} &= -\log[\text{OH}^-] \\ &= -\log[3.9864] \\ &= -0.6 \end{aligned}$$

$$\begin{aligned} \text{Require pH} &= 14 - \text{pOH} \\ &= 14 - (-0.6) \\ &= 14.6 \end{aligned}$$

APPENDIX H: Calculation on Pulse Chemisorption Results

The formulas from Table 2.4 were used to calculate the metal dispersion, D, metal surface area, A and metal average particle size, d_p .

Sample Calculation on Dry Impregnation Ni-Fe Catalyst

Fraction of nickel on support = 0.543

Fraction of iron on support = 0.457

Atomic radius of nickel = 149 pm
= 0.149 nm

Atomic radius of nickel = 156 pm
= 0.156 nm

Nickel cross-sectional area = $\pi \times (0.149\text{nm})^2$
= 0.06975 nm²/atom

Iron cross-sectional area = $\pi \times (0.156\text{nm})^2$
= 0.07645 nm²/atom

Volume of gas adsorbed = $1.44 \times 10^{-5} \frac{\text{mol}}{\text{g catalyst}}$

Amount of metals loaded = 0.2252 g metal/g catalyst

Gas adsorbed per gram of metal = $\frac{1.44 \times \frac{10^{-5} \text{mol}}{\text{g catalyst}}}{0.2252 \text{ g metal/g catalyst}}$
= $6.41 \times 10^{-5} \frac{\text{mol}}{\text{g metal}}$
= $64.1 \frac{\mu\text{mol}}{\text{g metal}}$

$$\begin{aligned}
 \text{Moles of metal on surface} &= n \times V_{\text{adsorbed}} \\
 &= 2 \times 1.44 \times 10^{-5} \text{ mol/g} \\
 &= 2.88 \times 10^{-5} \text{ mol/g}
 \end{aligned}$$

$$\begin{aligned}
 \text{Average MW of Ni-Fe} &= \left(58.7 \frac{\text{g}}{\text{mol}} \times 0.543 \right) + \left(55.845 \frac{\text{g}}{\text{mol}} \times 0.457 \right) \\
 &= 57.4 \text{ g/mol}
 \end{aligned}$$

$$\begin{aligned}
 \text{Moles of metal in sample} &= \frac{M}{\text{mw} \times 100} \\
 &= \frac{0.2252}{57.4 \times 100} \text{ mol/g} \\
 &= 0.00392 \text{ mol/g}
 \end{aligned}$$

$$\begin{aligned}
 \text{Metal dispersion, } \mathbf{D} &= \frac{2.88 \times 10^{-5} \text{ mol/g}}{0.00392 \text{ mol/g}} \times 100\% \\
 &= 0.74\%
 \end{aligned}$$

$$\begin{aligned}
 \text{Surface area of nickel on catalyst} &= \text{mole of nickel on surface} \times N_A \times a \\
 &= \left(2.88 \times 10^{-5} \frac{\text{mol metal}}{\text{g}} \times 0.543 \frac{\text{mol Ni}}{\text{mol metal}} \right) \\
 &\quad \times 6.022 \times 10^{23} \frac{\text{atom}}{\text{mol}} \times 0.06975 \frac{\text{nm}^2}{\text{atom Ni}} \\
 &= 6.58 \times 10^{17} \frac{\text{nm}^2}{\text{g}}
 \end{aligned}$$

$$\begin{aligned}
 \text{Surface area of iron on catalyst} &= \text{mole of iron on surface} \times N_A \times a \\
 &= 2.88 \times 10^{-5} \frac{\text{mol metal}}{\text{g}} \times 0.457 \frac{\text{mol Fe}}{\text{mol metal}} \\
 &\quad \times 6.022 \times 10^{23} \frac{\text{atom}}{\text{mol}} \times 0.07645 \frac{\text{nm}^2}{\text{atom Fe}} \\
 &= 6.07 \times 10^{17} \frac{\text{nm}^2}{\text{g}}
 \end{aligned}$$

$$\begin{aligned}
 \text{Total metal surface area, } \mathbf{A}_m &= 6.58 \times 10^{17} \frac{\text{nm}^2}{\text{g}} + 6.07 \times 10^{17} \frac{\text{nm}^2}{\text{g}} \\
 &= 1.26 \times 10^{18} \frac{\text{nm}^2}{\text{g}} \\
 &= 1.26 \frac{\text{m}^2}{\text{g}}
 \end{aligned}$$

$$\begin{aligned} \text{Surface area per nickel atom, } a_{Ni} &= \frac{6.58 \times 10^{17} \frac{\text{nm}^2 \text{Ni}}{\text{g}}}{2.88 \times 10^{-5} \frac{\text{mol metal}}{\text{g}} \times 6.022 \times 10^{23} \frac{\text{atom}}{\text{mol}}} \\ &= 3.79 \times 10^{-2} \frac{\text{nm}^2}{\text{Ni atom}} \end{aligned}$$

$$\begin{aligned} \text{Surface area per iron atom, } a_{Fe} &= \frac{6.07 \times 10^{17} \frac{\text{nm}^2 \text{Ni}}{\text{g}}}{2.88 \times 10^{-5} \frac{\text{mol metal}}{\text{g}} \times 6.022 \times 10^{23} \frac{\text{atom}}{\text{mol}}} \\ &= 3.49 \times 10^{-2} \frac{\text{nm}^2}{\text{Ni atom}} \end{aligned}$$

$$\begin{aligned} \text{Atomic volume of nickel, } V_{Ni} &= \frac{\text{atomic weight}}{\rho N_A} \\ &= \frac{58.7 \frac{\text{g}}{\text{mol}}}{8.9 \frac{\text{g}}{\text{cm}^3} \times 6.022 \times 10^{23} \frac{\text{atom}}{\text{mol}}} \times \frac{10^{21} \text{cm}^3}{\text{nm}^3} \\ &= 0.011 \text{ nm}^3 \end{aligned}$$

$$\begin{aligned} \text{Atomic volume of iron, } V_{Fe} &= \frac{\text{atomic weight}}{\rho N_A} \\ &= \frac{55.845 \frac{\text{g}}{\text{mol}}}{7.87 \frac{\text{g}}{\text{cm}^3} \times 6.022 \times 10^{23} \frac{\text{atom}}{\text{mol}}} \times \frac{10^{21} \text{cm}^3}{\text{nm}^3} \\ &= 0.0118 \text{ nm}^3 \end{aligned}$$

$$\begin{aligned} \text{Average nickel particle size} &= 6 \times \frac{V_{Ni}/a_{Ni}}{D} \\ &= 6 \times \frac{0.011/3.79 \times 10^{-2}}{0.0074} \\ &= 235.95 \text{ nm/atom} \end{aligned}$$

$$\begin{aligned} \text{Average iron particle size} &= 6 \times \frac{V_{Fe}/a_{Fe}}{D} \\ &= 6 \times \frac{0.0118/3.49 \times 10^{-2}}{0.0074} \\ &= 275.20 \text{ nm/atom} \end{aligned}$$

Table H.1: Amount of Gas Adsorbed per gram of Metal.

Catalyst Type	V_{adsorbed} (mol/g catalyst)	Amount of metal loaded (g metal/g catalyst)	Gas adsorbed per gram of metal loaded (mol/g metal)	Gas adsorbed per gram of metal loaded (μmol/g metal)
A	8.13E-05	0.79	1.03E-04	102.87
B	6.66E-05	0.74	8.98E-05	89.76
C	4.60E-05	0.37	1.25E-04	124.59
CP Ni-Fe	1.21E-04	0.74	1.64E-04	163.95
CP Ni-Zn	1.24E-04	0.81	1.52E-04	152.50
DI Ni-Fe	1.44E-05	0.23	6.41E-05	64.06
DI Ni-Zn	7.52E-06	0.19	3.94E-05	39.38
CP Ni	1.77E-05	0.23	7.68E-05	76.78

Table H.2: Metal Dispersion.

Catalyst Type	V_{adsorbed} (mol/g)	Metal present on surface (mol/g)	Metal loading (wt%)	MW (g/mol)	Total metal in sample (mol/g)	Dispersion (%)
A	8.13E-05	1.63E-04	79.02	58.69	1.35E-02	1.21
B	6.66E-05	1.33E-04	74.14	58.69	1.26E-02	1.05
C	4.60E-05	9.21E-05	36.95	58.69	6.29E-03	1.46
CP Ni-Fe	1.21E-04	2.41E-04	73.62	57.13	1.29E-02	1.87
CP Ni-Zn	1.24E-04	2.48E-04	81.31	61.71	1.32E-02	1.88
DI Ni-Fe	1.44E-05	2.88E-05	22.52	57.39	3.92E-03	0.74
DI Ni-Zn	7.52E-06	1.50E-05	19.10	61.82	3.09E-03	0.49
CP Ni	1.77E-05	3.53E-05	22.70	58.69	3.87E-03	0.91

Table H.3: Metal Surface Area.Note: Cross sectional $\text{Area}_{\text{Ni}} = 0.06975 \text{ nm}^2/\text{atom}$;Cross sectional $\text{Area}_{\text{Ni}} = 0.07645 \text{ nm}^2/\text{atom}$

Catalyst Type	Metal Present on surface (mol/g)	Metal surface atoms (atom/g)	Ni Surface Area (nm^2/g)	Fe or Zn surface area (nm^2/g)	Metal surface area (nm^2/g)	Metal surface area (m^2/g)
A	1.63E-04	9.79E+19	-	-	6.83E+18	6.83
B	1.33E-04	8.01E+19	-	-	5.59E+18	5.59
C	9.21E-05	5.54E+19	-	-	3.87E+18	3.87
CP Ni-Fe	2.41E-04	1.45E+20	4.57E+18	6.10E+18	1.07E+19	10.67
CP Ni-Zn	2.48E-04	1.49E+20	5.72E+18	4.26E+18	9.98E+18	9.98
DI Ni-Fe	2.88E-05	1.74E+19	6.58E+17	6.07E+17	1.26E+18	1.26
DI Ni-Zn	1.50E-05	9.05E+18	3.36E+17	2.68E+17	6.04E+17	0.60
CP Ni	3.53E-05	2.13E+19	-	-	1.48E+18	1.48

Table H.4: Metal Average Particle Size.Note: $V_{\text{Ni}} = 0.0110 \text{ nm}^3$; $V_{\text{Fe}} = 0.0118 \text{ nm}^3$; $V_{\text{Zn}} = 0.0152 \text{ nm}^3$

Type	Ni fraction	Fe or Zn fraction	a_{Ni} ($\frac{\text{nm}^2}{\text{atom}}$)	a_{Fe} ($\frac{\text{nm}^2}{\text{atom}}$)	D	Average Ni particle size ($\frac{\text{nm}}{\text{atom}}$)	Ave Fe or Zn particle size ($\frac{\text{nm}}{\text{atom}}$)
A	-	-	0.0697	-	1.21E-02	78.02	-
B	-	-	0.0697	-	1.05E-02	89.41	-
C	-	-	0.0697	-	1.46E-02	64.41	-
CP Ni-Fe	0.451	0.549	0.0315	0.0420	1.87E-02	111.45	89.96
CP Ni-Zn	0.550	0.450	0.0383	0.0285	1.88E-02	91.08	170.05
DI Ni-Fe	0.543	0.457	0.0379	0.0349	7.35E-03	235.95	275.20
DI Ni-Zn	0.533	0.467	0.0371	0.0296	4.87E-03	363.33	633.35
CP Ni	-	-	0.0697	-	9.13E-03	103.16	-

APPENDIX I: Average Elemental Composition from SEM-EDX

Table I.1: Average Weight Percent of Metal Loadings.

	Spot A			Spot B			Spot C			Average		
CP Ni-Fe	Fe	Ni	Total	Fe	Ni	Total	Fe	Ni	Total	Fe	Ni	Total
	39.54	32.16	71.7	40.5	33.32	73.82	41.15	34.18	75.33	40.40	33.22	73.62
fraction	0.551	0.449	1.000	0.549	0.451	1.000	0.546	0.454	1.000	0.549	0.451	1.000
CP Ni-Zn	Zn	Ni	Total	Zn	Ni	Total	Zn	Ni	Total	Zn	Ni	Total
	35.34	43.47	78.81	37.75	46.63	84.38	36.78	43.96	80.74	36.62	44.69	81.31
fraction	0.448	0.552	1.000	0.447	0.553	1.000	0.456	0.544	1.000	0.450	0.550	1.000
DI Ni-Fe	Fe	Ni	Total	Fe	Ni	Total	Fe	Ni	Total	Fe	Ni	Total
	17.07	11.92	28.99	6.08	9.39	15.47	7.72	15.37	23.09	10.29	12.23	22.52
fraction	0.589	0.411	1.000	0.393	0.607	1.000	0.334	0.666	1.000	0.457	0.543	1.000
DI Ni-Zn	Zn	Ni	Total	Zn	Ni	Total	Zn	Ni	Total	Zn	Ni	Total
	9.86	10.95	20.81	8.47	9.51	17.98	8.45	10.05	18.5	8.93	10.17	19.10
fraction	0.474	0.526	1.000	0.471	0.529	1.000	0.457	0.543	1.000	0.467	0.533	1.000

APPENDIX J: Raw Data of Characterisation Analyses

ICP-OES RAW DATA

XRD RAW DATA

TPR RAW DATA

PULSE CHEMISORPTION
RAW DATA

EDX RAW DATA

APPENDIX K: Material Safety Data Sheet